Thank you for the constructive comments and suggestions regarding our manuscript "*Deep Circulation in the South China Sea Simulated in a Regional Model*" [paper No.: os-2019-29]. The revised manuscript is attached. All the comments have been considered. Below are the detailed responses (in black) to the reviewer's comments (in blue).

Anonymous Referee #2

Review of "Deep Circulation in the South China Sea Simulated in a Regional Model" Zhao et al. presented a numerical study on the spatial characteristics of the deep western boundary currents (WBCs) in the South China Sea (SCS), using an eddyresolving configuration of HYCOM. They addressed the role of Pacific overflow water and enhanced diapycnal mixing in studying the dynamics of the WBCs. The study provides some quantitative model diagnosis which could be useful to the relevant research community, however, I am not convinced that this work brings further insight into understanding the dynamics of WBCs in general or specifically in the SCS, and therefore has limited contribution to advancing the science for this topic. The simulations are more like a model exercise on idealized vertical mixing, although the authors have been trying to compare their results to observations and previous model studies. Many numbers quantified and conclusions drawn seem to merely confirm what has been found before in the literature. In my opinion, this work to some extent also suffers from flawed methodology, inadequate discussion/analysis, missing information, and poor presentation of figures.

I acknowledge the efforts that the authors have put and the potential value of the topic, but I have to recommend rejection of the manuscript with its current status. Some overall and more specific comments are as follows.

[#1] Referee Comment: 1) model configuration (method): I am not convinced that the authors can make any meaningful quantification of the WBCs, nor any one-to-one comparison with observations, without surface forcing and with closed open boundaries. ". . . evidence of surface forcing to the deep layer dynamics has not yet been found" is not a good argument, and does not necessarily mean that surface forcing is not important. It is possible that the role of the surface forcing is not as important as the overflow inflow at Luzon Strait (LS), but it remains unknown unless some sensitivity experiments are carried out to test it. Similarly, ocean circulations in the LS and SCS are highly interactive with circulations in the western Pacific. Although T/S are relaxed at the open boundaries, but without inflow from the Equatorial Pacific and outflow leaving the model domain in the north (e.g. Kuroshio), how would this affect the analysis and quantified properties of the deep WBCs in this work?

If too much work for implementing or turning on the surface forcing and open boundaries, the authors should at least make clear of the limitations in the manuscript, and/or discuss how this could potentially affect their simulation results.

Furthermore, I am also not convinced by the approach the authors did with enhanced mixing. a) The configuration of enhanced mixing is still highly idealized compared to the observations compiled by Yang et al. (2016), which showed an inhomogeneous distribution of diapycnal mixing in the zonal, meridional, and vertical directions. For example, the vertical mixing in the northern SCS and near the bottom is much larger (up to 10^-2). I am not saying the model setup is wrong, but I think the authors should add more discussions on this point, and make clear of the caveat and idealized nature of their model setup. b) the two hot spots with enhanced mixing, separated by a narrow band of low mixing in

the model seems bizarre to me; would it make any difference if this narrow band is also filled with high mixing? There actually seems a lack of observations within this band in the observations of Yang et al.

Author's response: The reviewer's concern is reasonable and is worth to be profoundly investigated. In the manuscript, we clarify these limitations of the current model in the last section as follows, "It is noteworthy that despite reasonable agreement between the current simulation and observations, surface forcing, which have potential impact on the modification of ocean stratification and the deep circulation (e.g., Su et al., 2014, 2016a, 2016b; Yang et al., 2015), is not applied to the numerical experiments. Although configured with a buffer zone near the eastern boundary, the experiments are currently configured with closed lateral boundary condition, which cannot simulate the interactions between the processes of the current model domain and the Pacific/Indonesia seas. These limitations may introduce uncertainty to some extent to the simulation results in this study. The potential impact of surface forcing and boundary conditions on the deep circulation in the SCS is worth to be investigated." (lines 299-306)

As for the enhanced mixing configured to the experiments, we followed the results of Yang et al. (2016). We agree that hundreds of profiles and parameterization method are not sufficient to quantitively accurately present the three-dimensional structure of mixing in the SCS. However, the two mixing ''hotspots'' indicated by the study could be qualitatively robust and consistent with the mechanism of dissipation of internal tides. Therefore, in the current study, instead of applying the exact three-dimensional results of mixing calculated by Yang et al. (2016), we configured the experiments with somehow idealized mixing scheme as far as reflecting the two mixing "hotspots". We clarify the limitations of these configurations to be more specific. (lines 156-161)

Changes in manuscript: We rephrased the sentence and discussed the limitations of no surface forcing and the enhanced mixing in the model configuration of the manuscript.

[#2] Referee Comment: 2) Model spin-up and validation I do not see sufficient validation and assessment of the simulation. A comparison of velocity cross-section with observations (e.g. Fig. 2 only) provides very limited support on the robustness of the simulation results. For instance, how does the model perform in simulating the T/S properties in general for the SCS (at least for the mid- and deep ocean, if not for the whole depth)? Importantly, as the authors deem the dense overflow at the LS to be a crucial factor in determining the dynamics of the WBCs, how is the model behaving in simulating the overflow at the strait? e.g. are the T/S/rho properties of the overflow captured? Are they descending to the bottom basin without being (numerically) diffused? The authors mentioned some numbers on the volume transport of the overflow, but how is the overflow defined?

Besides, regarding the model-data comparison (Fig. 2), "As expected, the control run shows reasonable agreement with the cross-section observations" (L171) seems like an overstatement to me. The WBCs and the return flow are clearly stronger with a broader core compared to the observations. This inconsistency and the possible reasons are not adequately addressed.

As for the model spin-up, the authors need to justify that 20 years are long enough for the model to reach equilibrium or quasi-equilibrium. Evidence should be shown; examples are timeseries of volume transport of the Pacific overflow and the deep WBCs, timeseries of deep basin T/S, and so on.

Author's response: Thanks for this suggestion.

For now, the published and accessible observational data in the deep SCS is relatively sparse. This somehow results to the discrepancy between different climatology atlases, like the WOD01 and GDEM, which are based on different interpolation methods. Both atlases have been used to investigate the deep circulation in the SCS (Fig. RC1, Qu et al., 2006a; Wang et al., 2011). However, the T/S spatial structure of the deep SCS shown in these studies were notably different. Therefore, we did not use these atlases for the model validation. As the key branch of deep circulation, DWBC is the most dominating feature with enhanced velocity and energetic variability. The recent year-long mooring observation on the DWBC in the SCS (Zhou et al., 2017) provides an ideal result for assessing the model simulation. Besides, as the only origin of deep water in the SCS, deepwater overflow through the Luzon Strait have been studied by a series of works, especially on its volume transport. This provides another key result for the assessment of model simulation. Except these two aspects, we do not find other observation results appropriate for validation of model for now. It would be appreciated if the reviewer could provide or suggest where to find more data for the validation.

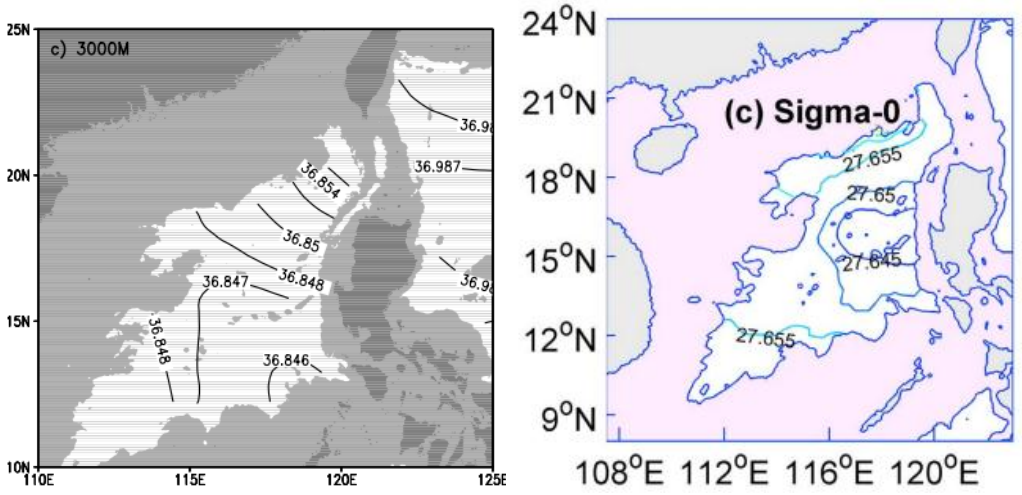

Figure RC1. Potential density calculated from the synthetic salinity at 3000 m in the deep South China Sea. The left panel shows σ_2 based on WOD01 (Qu et al., 2006a) and the right panel shows σ_0 based on GDEM (Wang et al., 2011).

In this work, to be consistent and comparable with Zhao et al. (2014), the transport across 121 ℃E and from the 25th layer (corresponding to σ_2=36.82 kg m^{-3}) to bottom is calculated as the total transport of the deepwater overflow in the Luzon Strait.

The simulated DWBC (4 cm s^{-1}) and recirculation are stronger than the observations (2 cm s^{-1}) probably due to that the simulated source (1.2 Sv), deepwater overflow in the Luzon Strait, is slightly stronger than the observations (0.88 Sv; Zhou et al., 2014). We noted this in Section 3.1. (lines 183-186)

Fig. RC2 shows the section view of year-mean thickness structure at zonal and meridional section for the control run. The thickness structure was basically stable in the last five years indicated the control run obtained a steady state of the deep circulation in the SCS.

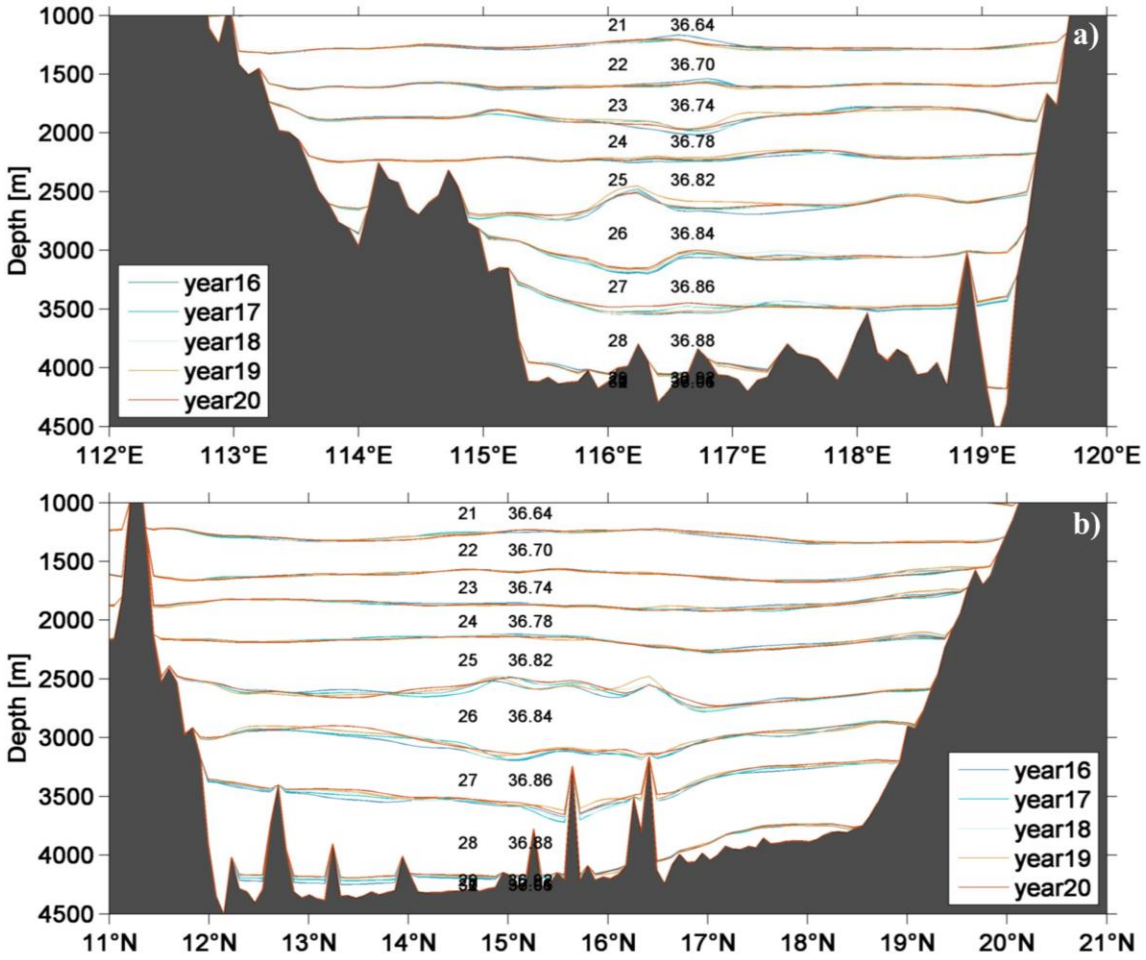

Figure RC2. Section view of year-mean thickness structure at a zonal section of 16.5 ℃N (a) and a meridional section of 116 ℃E (b) for the control run. Thickness numbers and density referenced to 2000 m (σ_2, kg m^{-3}) are indicated.

Changes in manuscript: We added figure and description to clarify this. (lines 163-164)

Minor comments.

[#3] > L9: the first sentence does not need to and should not appear in the abstract;

Author's response: Corrected. (line 9)

[#4]> L35-37: just to clarify, the 'three-dimensional circulation' is one component of the SCS throughflow, and it is the latter that serves as a heat/freshwater conveyor, right?

Author's response: The "South China Sea Throughflow" is another saying of the "three-dimensional circulation" here. We revise the sentence in case of ambiguity. (line 36)

[#5]> L38-52: while the topic of this work is on the SCS deep WBCs, the authors use lots of space introducing the overflow at the LS (I do understand that the WBCs are strongly linked with the overflow). The authors could consider reducing this part.

On the other hand, having given so much background information on the overflow, the authors are expected to describe a bit more on the model representation of overflows, other than merely giving a

number of volume transport. See also my earlier comment 2).

Author's response: Following the comment, we reduced the introduction on the deepwater overflow in the manuscript. As for the model representation of overflows, previous study with similar model configurations (Zhao et al., 2014) has investigated the deepwater overflow in the Luzon Strait more detailly. Therefore, we focus on the deep circulation inside the SCS deep basin and may not involve the overflow in detail. (lines 47-53)

[#6]> L41-44: the geographical locations are challenging to the readers. The authors could consider avoiding this, or provide a map showing their locations.

Author's response: We now note the locations of the Bashi Channel, the Luzon Trough and the Taltung Canyon in Fig. 1.

[#7]> L46: rms – full name should be given here.

Author's response: Thanks and corrected as root mean square. (line 47)

[#8]> L68-69: ‘: : : and higher resolution’ – how much higher? e.g. slightly higher than 0.4/0.5 degree, or as high as the resolution in this study?

Author's response: We now note the resolution in She et al. (2014) and Xu and Oey (2014) is 1/12 °and 1/12 °, respectively. (line 70)

[#9]> L71: what is a/the ‘north deep circulation’?

Author's response: We revised the words to be “a stronger deep boundary current along the northern continental slope”. (lines 72-73)

[#10]> L76: “Since the DWBC is due to the LS overflow and the beta effect” – this assertion appears to come out of the blue; is this very well known already? Any reference?

Author's response: We rephrase the sentence and add the corresponding references. (lines 78-79)

[#11]> L77: To me the resolution is a secondary consideration. Whether the model produces sufficient overflow water that spills over the sill and whether the water can descend down to the bottom with proper entrainment en route are more important. This could well be my personal biased view though.

Author's response: We agreed that the overflow and the entrainment also play an important role in the deep circulation in the SCS. A short sentence has been added to the text to mention this point. (lines 81-82)

[#12]> L81: I don’t see the logical connection between “Due to the lack of field observations” and the rest of the sentence.

Author's response: We rephrased the sentence to avoid being ambiguity. (lines 84-85)

Deep Circulation in the South China Sea Simulated in a Regional Model

Xiaolong Zhao[1,2], Chun Zhou[2], Xiaobiao Xu[3], Ruijie Ye[2], Jiwei Tian[2] and Wei Zhao[2]

[1]North China Sea Marine Forecasting Center, State Oceanic Administration, Qingdao, 266061, P. R. China.
[2]Key Laboratory of Physical Oceanography/CIMST, Ocean University of China and Qingdao National Laboratory for Marine Science and Technology, Qingdao 266100, P. R. China.
[3]Center for Ocean-Atmospheric Prediction Studies (COAPS), Florida State University, Tallahassee, FL, USA.

Correspondence to: ~~Wei Zhao~~Chun Zhou (~~weizhao~~chunzhou@ouc.edu.cn)

Abstract. ~~The South China Sea (SCS) is the largest marginal sea in the northwest Pacific Ocean.~~ In this study, deep circulation in the ~~SCS~~South China Sea (SCS) is investigated using results from mesoscale-eddy-resolving, regional simulations using the Hybrid Coordinate Ocean Model (HYCOM) verified by continuous current-meter observations. Analysis of these results provides a detailed spatial structure and temporal variability of the deep circulation in the SCS. The major features of the SCS deep circulation are a basin-scale cyclonic gyre and a concentrated deep western boundary current (DWBC). Transport of the DWBC is ~2 Sv at 16.5 ℃N with a width of ~53 km. Flowing southwestward, the narrow DWBC becomes weaker with a wider range. The model results reveal the existence of 80- to 120-day oscillation in the deep northeastern circulation and the DWBC, which are also the areas with elevated eddy kinetic energy. This intraseasonal oscillation propagates northwestward with a velocity amplitude of ~1.0 to 1.5 cm s^{-1}. The distribution of mixing parameters in the deep SCS plays a role in both spatial structure and volume transport of the deep circulation. Compared with the northern shelf of the SCS with the Luzon Strait, deep circulation in the SCS is more sensitive to the large vertical mixing parameters of the Zhongsha Island Chain area.

1. Introduction

The South China Sea (SCS, Fig. 1) is the largest marginal sea in the Southeast Asian Waters, with an area of approximately 3.5×10^6 km^2 and a depth exceeding 4000 m in the central basin (Wyrtki, 1961). It is connected to the surrounding waters mostly by shallow straits: ~~The~~ Taiwan Strait to the East China Sea in the north, the Karimata Strait to the Java Sea in the south, and the Mindoro Strait to the Sulu Sea in the southeast. The 355 km-wide Luzon Strait, with a sill depth of ~2400 m, is the only deep connection between the SCS and its ambient oceans. There, cold and salty (thus dense) North Pacific Deep Water (NPDW, with potential temperature and salinity of ~1.79 ℃ and 34.64 psu; Mantyla, 1975; Zhao et al., 2016) penetrates the SCS basin through the deepwater overflow in the Luzon Strait driven by the baroclinic pressure gradient between the Pacific Ocean and the SCS (Qu et al., 2006a; Zhao et al., 2014; Zhou et al., 2014, 2018). Since the SCS is closed below 2400 m, the incoming NPDW eventually

upwells as a result of enhanced mixing (~10^{-3} m^2 s^{-1}; Tian et al., 2009; Alford et al., 2011; Yang et al., 2016) and exits the SCS either in the intermediate layer through the Luzon Strait back to the Pacific Ocean (Chao et al., 1996; Chen and Huang, 1996; Li and Qu, 2006; Qu et al., 2000; Tian et al., 2006; Zhang et al., 2015; Gan et al., 2016) or in the upper layer through several shallow straits in the southern part of the SCS to the Java and Sulu Seas (e.g., Qu et al., 2009; Yaremchuk et al., 2009). This three-dimensional circulation ~~constitutes~~, also known as the SCS throughflow (Qu et al., 2006b), serving as a heat and freshwater conveyor that is climatologically important on regional and global scales (e.g., Gordon et al., 2012).

As a key element of the SCS circulation, the deepwater overflow through the Luzon Strait has been observed in a number of studies (e.g., Wang, 1986; Liu and Liu, 1988; Qu et al., 2006a; Song, 2006; Tian et al., 2006; Chang et al., 2010; Yang et al., 2010, 2011; Tian and Qu, 2012; Zhao et al., 2014; Zhou et al., 2014; Zhao et al., 2016; Ye et al., 2019), and its volume transport, temporal variability, as well as the water properties are now relatively well defined. Based on data from moorings deployed at two locations for 3.5 years, Zhou et al. (2014) estimated a mean transport of 0.83 Sv (1 Sv = 10^6 m^3 s^{-1}) in the Bashi Channel and 0.88 Sv further downstream in the Luzon Trough (which includes some additional minor contribution through the Taltung Canyon north of the Bashi Channel). More recently, Zhao et al. (2016) used results from ten current meters at three mooring locations in the Bashi Channel and estimated a similar eight-month mean transport of 0.78 Sv (with a total ~~rms~~root mean square error of 0.18 Sv). ~~The overflow transport exhibits a significant seasonal variability (with a higher transport in October-December and a lower transport in March-May), corresponding well with the seasonal variation of the density difference between the SCS and the Pacific Ocean close to the sill depth (Zhou et al., 2014) and a significant intraseasonal variability on a near-30-day timescale, which is close to the resonance period of the deep channel in the Luzon Strait (Zhao et al., 2016). The time series from 2009 to 2013 indicates an interannual variability, but longer observations are needed to determine long-term variability.~~

~~Compared to the deepwater overflow in the Luzon Strait~~Comparatively, much less is known about the deep circulation in the SCS. In general, a cyclonic circulation with an intensified deep western boundary current (DWBC) is expected, following the classical Stommel-Arons abyssal circulation theory (Stommel and Arons, 1960a, 1960b). The temperature, salinity, and tracer distributions of the World Ocean Database 2001 indicate such a cyclonic circulation in the deep SCS (Qu et al., 2006a). A similar basin-scale cyclonic circulation, with an estimated mean transport of 3.0 Sv, is suggested by Wang et al. (2011) based on an analysis of the ocean climatology database, the

Generalized Digital Environment Model (GDEM; Carnes, 2009). Recently, an array of six current meter moorings was deployed off the eastern slope of the Zhongsha Islands from August 2012 to January 2014 (Zhou et al., 2017). Results from these direct measurements show, for the first time, the existence of the DWBC in the deep SCS basin, with a volume transport of 1.65 Sv and high temporal variability around 90 days. This mooring array in Zhou et al. (2017) is used in the present study.

Numerical models are also used to study the deep circulation in the SCS. Chao et al. (1996) using a 0.4° three-dimensional, climatology-driven circulation model show a deep cyclonic circulation in the deep SCS but without clear DWBC. Lan et al. (2013, 2015), based on results of 0.5° simulations, suggest that the basin-scale deep circulation is controlled by the deep overflow from Luzon Strait. In their simulation, a basin-scale cyclonic gyre is prominent during July-September and hardly identified during January-March. With data assimilation and higher resolution (1/12° and 1/10°, respectively), Shu et al. (2014) and Xu and Oey (2014) show a complicated three-layer circulation in the SCS, cyclonic in the upper layer, anticyclonic in the middle, and cyclonic in the deep. With 1/12° MITgcm, Wang et al. (2017) simulated a stronger ~~north~~ deep ~~circulation~~ boundary current along the northern continental slope comparable with the DWBC. Earlier simulating studies indeed indicated the general cyclonic pattern of the deep SCS circulation and the existence of the DWBC. However, numerous discrepancies exist among different simulation results: First, the accurate location of the DWBC is controversial. For example, Lan et al. (2013, 2015) simulated deep circulation flows southwestward off the western slope of the Zhongsha Islands, while Shu et al. (2014) and Xu and Oey (2014) indicated the DWBC flows off the eastern slope of the Zhongsha Islands. Since the DWBC ~~is~~ could be due to the Luzon Strait overflow and the β effect (e.g., Lan et al., 2013; Stommel and Arons, 1960a), whether the model horizontal resolution is sufficient to distinguish the deep Luzon Strait (~15 km wide at 2000 m depth, which is the time mean upper interface of the overflow, see Zhao et al., 2016) could be one of the reasons. Second, different models may have different performances on the entrainment and mixing of ambient water after the deepwater overflow spills into the deep SCS. Third, in most simulations there is a strong cyclonic or anticyclonic circulation cell at the southwest part of the deep circulation under week mixing: a separate cyclonic circulation in Chao et al. (1996) and Shu et al. (2014), while there is an anticyclonic one in Xu and Oey (2014). ~~Due to the lack of field observations, s~~Simulation results of the deep circulation in the SCS need to be verified based on observations before being employed to the discussion of the spatio-temporal characteristics of the deep circulation in the SCS.

With progresses on the dynamics of submesoscale processes and internal tides (e.g., Su et al., 2018; Yu et al., 2019; Polzin et al., 1996), abyssal enhanced mixing generated by these processes and its impact on the stratification and deep circulation has been drawn increasing attention. Enhanced mixing is a well-observed feature in the SCS. The observations of Tian et al. (2009) and Alford et al. (2011) show diapycnal diffusivity in the SCS and the Luzon Strait increases from about 10^{-3} m^2 s^{-1} at 1000 m to 10^{-2} m^2 s^{-1} near the sea floor. This is about two orders of magnitude higher than that in the North Pacific Ocean and is furnished by energetic internal waves induced by the prominent bathymetry in the Luzon Strait (Niwa and Hibiya, 2004; Jan et al., 2007; Tian et al., 2003, 2006). Based on hydrographic measurements with fine scale parameterizations from 335 stations (477 casts), Yang et al. (2016) recently obtained the three-dimensional distribution of turbulent mixing in the SCS for the first time. Two mixing "hotspots" were identified in the bottom waters in the northern shelf of the SCS with the Luzon Strait and the Zhongsha Island Chain areas (their Fig. 4), largely due to internal tide, bottom bathymetry, and near-inertial energy. Previous studies have shown enhanced mixing plays a role in deep circulation in both the Pacific Ocean and the Luzon Strait. Furue and Endoh (2005) indicated the deep Pacific Ocean diffusivity contributes to enhanced production of the Antarctic Bottom Water in the model. The northward transport of the deep meridional overturning circulation across the equator in the Pacific Ocean is stronger with the intense mixing than with weak mixing (Endoh and Hibiya, 2006; their Fig. 3). Zhao et al. (2014) suggested that enhanced mixing in the SCS and the Luzon Strait was the primary driving mechanism for the deep circulation in the Luzon Strait, since it is a key process responsible for the density difference between the Pacific Ocean and the SCS. Based on a simulated tidal mixing scheme, Wang et al. (2017) indicated the tide-induced diapycnal mixing in the Luzon Strait would have a negative effect on driving the cyclonic SCS deep circulation, although without the feature of two mixing "hotspots". Since the mixing is very strong and unevenly distributed in the deep SCS, it is necessary to modify the mixing scheme in the ocean model to be consistent with observed three-dimensional distribution of mixing. Nevertheless, previous numerical studies simulated the deep circulation with homogeneous or simulated vertical mixing parameters in the deep SCS, and one wonders about the sensitivity of the SCS deep circulation to the observed distribution of mixing.

~~Given the lack of observations and inadequate quality control, detailed structures of circulation in the deep SCS have not been mapped out and described adequately.~~ Combining the mooring array in Zhou et al. (2017) with results from mesoscale-eddy-resolving model simulations, the present study for the first time investigates deep circulation under ~~enhanced mixing~~ two mixing "hotspots" in the SCS. The paper is organized as follows. After the introduction,

the data and model configuration are described in Sect. 2. Section 3.1 presents the model results compared with observations. Section 3.2 is devoted to the horizontal pattern of mean circulation. Variability of deep circulation is discussed in Sect. 3.3, and Sect. 3.4 examines sensitivity to distribution of mixing. A summary and discussion follows in Sect. 4.

2. Data and Model Configuration

As part of the SCS mooring array, an array of six bottom-anchored moorings was deployed off the eastern slope of the Zhongsha Islands between 28 August 2012 and 11 January 2014 (M1-M6, see Fig. 1 for locations). Twenty-nine Aanderaa Data Instruments RCM Seaguard current meters were utilized to measure the horizontal current of the DWBC at nominal depths of 2000 m, 2500 m, 3000 m, 3500 m, and 4000 m, with generally 500 m resolution vertically. Details pertinent to these moorings are shown in Table 1. All current meters were configured to record data at a sample interval of one hour. Detailed results are discussed in Zhou et al. (2017). Here, we use the observed mean velocity section to examine the simulated time mean structure of the DWBC.

The regional simulation is similar to that of Zhao et al. (2014). The general circulation model used was the Hybrid Coordinate Ocean Model (HYCOM; Bleck, 2002; Chassignet et al., 2003) configured with a horizontal resolution of 1/12 ° (~9 km resolution in our area of interest). The computational domain, which extends from 4 °N to 25 °N and 105 °E to 125 °E (Fig. 1), includes the SCS and part of the northwestern Pacific Ocean. A total of 32 vertical hybrid layers are configured with density referenced to 2000 m (σ_2, kg m^{-3}): 28.10, 28.90, 29.70, 30.50, 30.95, 31.50, 32.05, 32.60, 33.15, 33.70, 34.25, 34.75, 35.15, 35.50, 35.80, 36.04, 36.20, 36.34, 36.46, 36.56, 36.64, 36.70, 36.74, 36.78, 36.82, 36.84, 36.86, 36.88, 36.92, 36.96, 37.01, and 37.06. The bottom topography is from version 13.1 of Smith and Sandwell (1997) with ~~1'~~1/60 ° resolution. The simulation was initialized with rest and January temperature and salinity fields from the third version of monthly 1/4 °ocean climatology GDEM (Carnes, 2009). ~~Despite the fact that surface forcing is significant in this region as regulating the upper layer circulation, evidence of surface forcing to the deep layer dynamics has not yet been found.~~ Since the current work is designed to be a process study, surface forcing was not applied in the experiments. All lateral boundaries were closed with no normal flow, within a 19-grid buffer zone near the eastern boundary, the modeled temperature and salinity are restored toward the same (monthly) climatology with an e-folding time of 0.5-32 days that increased with distance from the boundary. The bottom stress was parameterized using a quadratic drag law at the lowest 10 m, with a constant drag coefficient $C_D = 2.5 \times 10^{-3}$.

Based on similar configurations with all of the numerical experiments started from rest and integrated for 10 years, Zhao et al. (2014) studied the deep water circulation in the Luzon Strait, which was in good agreement with the observations based on repeated conductivity-temperature-depth (CTD) and lowered acoustic Doppler current profiler (LADCP) surveys. We modified the K-profile parameterization (KPP; Large et al., 1994) mixing scheme in accordance with the two observed mixing "hotspots" found in Yang et al. (2016). Thus, the control run was configured with larger vertical mixing parameters, in which the diapycnal diffusivity beneath 1000 m were set to 10^{-3} m^2 s^{-1} in both the north shelf of the SCS with the Luzon Strait (109-122 °E, 18-23 °N) and the Zhongsha Island Chain area (109-122 °E, 14-17 °N, red boxes in Fig. 1). To examine the impact of mixing, four sensitivity experiments were used with the same configuration as the control run, but with different mixing schemes: Following Zhao et al. (2014), Exp-5 and Exp-3 were configured with the native KPP scheme as background mixing of 10^{-5} m^2 s^{-1} and the diapycnal diffusivity beneath 1000 m in the SCS and the Luzon Strait (west of 122 °E) as 10^{-3} m^2 s^{-1}, respectively. Exp-3A and Exp-3C were configured with the lager vertical mixing parameters in different areas, in which the diapycnal diffusivity beneath 1000 m were set to 10^{-3} m^2 s^{-1} in the north shelf of the SCS with the Luzon Strait (109-122 °E, 18-23 °N) and the Zhongsha Island Chain area (109-122 °E, 14-17 °N), respectively. Instead of applying the exact results of mixing distribution of Yang et al. (2016), these configurations are idealized to some extent, in order to reproduce the two mixing “hotspots” dynamically explained by dissipation of internal tides, while not following the specific distribution and magnitude which still need to be verified due to the limitations of numbers of CTD profiles and parameterization method. These configurations may somehow introduce uncertainty to the simulation results which is difficult to evaluate with the current observations.

In order to obtain a steady state of the deep circulation in the SCS, we integrated all of the numerical experiments for 20 years and averaged the last five years as the simulated annual mean results mentioned below (as shown in Fig. 2, the thickness structure was basically stable in the last five years indicated the control run has been stable ~~during the last 10 years~~).

3. Key Results

Observations from six moorings allow us to examine the simulate time mean structure of the DWBC and results from mesoscale-eddy-resolving model simulations are used to further investigate the structure and mechanisms of the deep circulation in the SCS.

3.1 DWBC in the SCS

Figure ~~2~~ 3 presents a comparison between the observed and simulated section view of the mean current in the deep western boundary of the SCS. Based on Zhou et al. (2017) and considering that the DWBC generally follows the topography, the observed current is re-coordinated into the cross-section, generally along the isobaths with positive direction pointing to the southwest. Observations at M5 and M6 are projected to the section (M1-M4). The simulated time-mean structure of velocity is a zonal section view of 15.4 °N for the control run close to these six moorings and indicated in the Fig. 1. Consistent with the observations, a bottom intensified current is simulated flowing southwestward off the eastern slope of the Zhongsha Islands. This is different from Lan et al. (2013, 2015) but similar with Shu et al. (2014) and Xu and Oey (2014). It appears that a horizontal resolution of 0.5 ° is not sufficient to resolve the deep Luzon Strait accurately, resulting in an inaccurate position of the DWBC in the simulation. The DWBC weakens upward, with its upper interface lying at around 2000 m. Horizontally, the model accurately reproduces the observed main axis of the DWBC (comparable with M1 and M2) and a recirculation (comparable with M4 an M5). The DWBC is ~100 km wide, with its core leaning on the slope of Zhongsha island. This modeled and observed DWBC is significantly narrower than Wang et al. (2011). Note that the simulated DWBC (4 cm s^{-1}) and recirculation are stronger than the observations (2 cm s^{-1}) since the source, deepwater overflow in the Luzon Strait, is the same status (1.2 to 0.8 Sv; Zhou et al., 2014; Zhao et al., 2016). As expected, the control run shows reasonable agreement with the cross-section observations.

3.2 Mean Circulation Pattern

To examine the simulated large-scale deep circulation in the SCS, we calculated the mean transports along four zonal sections (13.5 °N, 15.0 °N, 16.5 °N and 18.0 °N) of each layer including the 25th to 30th from 110 °E to 121 °E (Fig. ~~3~~4) for the control run. The cumulated transport of the 27th (σ_2=36.86 kg m^{-3}, ~3000-3500 m) layer shows a northward current in the southern part of the western boundary (near 114 °E in sections of 13.5 °N and 15.0 °N) that belongs to the anti-cyclonic middle layer of the SCS circulation (e.g., Gan et al., 2016; Shu et al., 2014; Xu and Oey, 2014), while the 28th (σ_2=36.88 kg m^{-3}, ~3500-4000 m) and 29th (σ_2=36.92 kg m^{-3}, ~4000-4200 m) layers show a consistent southward DWBC at different latitudes. The mean transport per unit width (in m^2 s^{-1}) from the 28th layer shows a strong deep cyclonic circulation in the SCS (Fig. ~~4a~~5a), and the 29th layer mostly presents the deep circulation in the Luzon Strait (Fig. ~~4b~~5b). Therefore, here we calculate the total mean transport per unit width ~~from~~ of the 28th ~~to~~and 29th layer to describe the pathway of deep circulation in the SCS (Fig. ~~5~~6).

The major features of the SCS deep circulation are a basin-scale cyclonic gyre and a western intensification. Driven by the baroclinic pressure gradient between the Pacific Ocean and the SCS in the Luzon Strait, deepwater overflow spills into the SCS mostly through two gaps in the Heng-Chun Ridge (as WG2 and WG3 in Zhao et al., 2014) along the 3800 m and 4000 m isobaths, respectively. With a confluence off the northern shelf, the current flows southwestward and then turns southward near 116 °E, 18 °N as an intensified DWBC along the eastern slope of the Zhongsha Islands. Restricted by the topography, the DWBC divides into two branches at 115 °E, 15.5 °N. A strong southwestward branch follows the western boundary southwestward and another goes southeastward near M4. The rest of the DWBC travels to the deep basin in the south and then turns northeastward into the middle basin, presenting a cyclonic pattern that makes the inflow water spread to nearly the entire SCS deep basin. We cumulated the mean transports along these four zonal sections from different layers to the 29th in order to quantitatively describe the deep circulation in the SCS (Fig. ~~6~~7). The volume transport of the DWBC is ~2.0 Sv at 16.5 °N (from the 27th to 29th layers) with a width of ~53 km, in agreement with the observed transport (1.65 Sv) and larger than the deepwater overflow in the Luzon Strait (1.2 Sv), which may be related to the entrainment of water from the interior ocean due to enhanced diapycnal mixing in the northeastern SCS (Tian et al., 2009; Yang et al., 2016). While flowing southwestward with an upwelling process, the DWBC becomes weaker and gets a wider range: Transport of the DWBC becomes ~1.2 Sv (from the 28th to 29th layers) with a width of ~140 km at 13.5 °N.

3.3 ~~Temporal~~ Intraseasonal Variability of the Deep Circulation

The model results reveal the existence of energetic intraseasonal variability in the SCS deep circulation. As shown in Fig. ~~7a~~8a, large eddy kinetic energy (EKE, defined as $0.5\times\left[(u-\bar{u})^2+(v-\bar{v})^2\right]$, where u and v are zonal and meridional velocities, respectively) areas appear in the deep northeastern circulation and the DWBC, indicating strong variability there. Topography, standing meanders, nonlocal energy propagation and turbulent energy cascade can intricate influence the EKE patterns (e.g., Su and Ingersoll, 2016). Periods of max power spectra density (PSD) indicate the dominant feature of the variability at the large EKE areas is an 80- to 120-day oscillation, based on spectrum analyze of zonal and meridional velocity time series from the 28th to 29th layers at each gird point for the control run (Fig. ~~8~~9). This oscillation also presents in the time series recorded by the six current-meter moorings M1-M6 deployed off the eastern slope of the Zhongsha Islands (Zhou et al., 2017). The relative leading time between the two closed cells in zonal and meridional directions can be obtained by calculating the lag correlation of

zonal and meridional velocity time series, respectively. Dividing the corresponding distance, we obtain the mean phase speed and direction of the deep oscillation (Fig. ~~7b~~8b). The waves show a northwestward propagation in both the deep northeastern circulation and the DWBC, with a velocity amplitude of ~1.0 to 1.5 cm s^{-1} (Fig. ~~7b~~8b), comparable with the mean speed of ~2.9 cm s^{-1} along the section M1-M6 (Zhou et al., 2017). Based on the principle axis variance ellipse of band-passed velocity and propagation direction, Zhou et al. (2017) suggested that the 80- to 120-day oscillation cannot be attributed to topographic Rossby waves, a mechanism for abyssal intraseasonal variability, especially at the deep western boundary (e.g., Thompson, 1977; Johns and Watts, 1986; Pickart and Watts, 1990; Hamilton, 2009). Other possibilities include the barotropic and baroclinic Rossby waves. In another sensitivity experiment we doubled the SCS basin and the 80- to 120-day oscillation peak disappeared, indicating this oscillation maybe related to the basin mode of the SCS (e.g., Platzman, 1972; Xu et al., 2007). This variability is a good topic for future studies.

3.4 Model Sensitivity to Distribution of Mixing

Exp-5, Exp-3, Exp-3A, and Exp-3C all show a basin-scale cyclonic gyre with a western intensification in the deep SCS (Fig. ~~9~~10). However, the volume transport of the deepwater overflow in the Luzon Strait, the DWBC, and the detail structure of the deep circulation are quite different in these experiments. The simulated deep circulation is much weaker in Exp-5 and Exp-3A (e.g., 0.9 and 1.0 Sv is smaller than the control run (1.2 Sv) of the overflow; 1.0 and 0.7 Sv are nearly two times smaller than the control run (2 Sv) at 16.5 ºN of the DWBC). On the other hand, it is closer to the control run in the Exp-3 and Exp-3C (1.4 and 1.2 Sv of the overflow; 2.2 and 1.9 Sv of the DWBC). Magnitude of upwelling is similar case: The upwelling transports southward from 16.5 ºN in Exp-5 and Exp-3A (0.6 and 0.6 Sv), two times smaller than the control run (1.2 Sv), while the control run, Exp-3 and Exp-3C are in reasonable agreement (1.2, 1.3 and 1.1 Sv). This indicates that compared with the north shelf of the SCS with the Luzon Strait, deep circulation in the SCS is more sensitive to the large vertical mixing parameters of the Zhongsha Island Chain area. This might be explained by the fact that the latter contains more areas of density difference, as the deep circulation is essentially density driven. With an increase in the range of strong mixing, the intensity of the deep circulation in the SCS is enhanced, suggesting that enhanced mixing in the SCS and the Luzon Strait plays an important role in maintaining the intensity of the SCS deep circulation. At the same time, the spatial structure of the deep circulation in the SCS also changes. For example, the southwest sub basin circulation is expanded in Exp-5, while the recirculation near the DWBC extends to the Zhongsha Island Chain area in the control run but not in the

other four experiments. By adjusting the thermohaline structure, enhanced mixing not only impacts the local deep circulation, but can also influence the deep circulation in other areas without enhanced mixing.

4. Summary and Discussion

Due to enhanced mixing in the deep SCS, the deep water in the SCS is expected to move upward much faster than deep water in the open ocean (on the order of 0.1 cm day^{-1}; e.g., Kunze et al., 2006). Qu et al. (2006a) gave an estimate of area-averaged vertical upwelling velocity of the deepwater in the SCS at $\omega=Q/A$=0.24 m d^{-1}, and applied a hydraulic theory to estimate the Luzon Strait transport Q=2.5 Sv and the area of the SCS at 2000 m to estimate as $A = 9\times10^{11}$ m^2. Based on long-term mooring observations, the upwelling velocity becomes 0.08 m d^{-1} while Q=0.8 Sv (Zhou et al., 2014; Zhao et al., 2016) in this way. Yang et al. (2016) obtained the vertical velocity as 0.32 m d^{-1} from a vertical advective-diffusive balance model based on the diffusivity results inferred from the Gregg-Henyey-Polzin parameterization and 0.28 m d^{-1} from a dynamically and kinematically consistent ocean state estimate system (Estimating the Circulation and Climate of the Ocean, ECCO; Forget et al, 2015). For the horizontal distribution of upwelling in the deep SCS basin, albeit without estimating the magnitude, Shu et al. (2014) indicated there are three northwest-southeast tilted zones where tracers upwell inferred from the modeled trajectories. These correspond to the three deep meridional overturning circulation cells. They speculated that one possible mechanism for these upwelling zones is the interaction between the topographically trapped waves on the slope and the westward planetary Rossby waves (e.g., Rhines, 1970; Anderson and Gill, 1975).

As described in Fig. ~~6d~~7d, the net transport of the 28th and 29th at these four sections are all southward, with the values decreasing as 1.25, 1.06, 0.77 and 0.42 Sv, respectively. This indicates the deep flow goes upward from the deep layer as a result of enhanced mixing in the deep SCS. By dividing the differences between the net transports with corresponding areas, the upward transports are found to be 0.19, 0.29, 0.35 and 0.42 Sv, which indicate the values of upwelling at each area are 0.19, 0.32, 0.27 and 0.22 m d^{-1}, respectively. We also cumulated the mean transports along four meridional sections (1.15 Sv at 118.5 °E, 0.88 Sv at 117.0 °E, 0.65 Sv at 115.5 °E and 0.29 Sv at 114.0 °E) and the corresponding upwelling became 0.28, 0.23, 0.36 and 0.29 m d^{-1}, respectively. This suggests that the DWBC is the strongest upwelling area. In order to present the horizontal distribution and magnitude of upwelling, we cumulated the diapycnal water mass transformation across the upper interface of the 28th layer for the control run in each 1 °×1 ° box (Fig. ~~10~~11). The upward transformation is due to interior diapycnal mixing and

elevations around the DWBC and seamounts areas with values of 1 m d^{-1} or larger, while downwelling exists in the relatively flat inner basin with values of 0.5 m d^{-1}. The magnitude of total diapycnal transformation of the SCS is close to that of the deepwater overflow in the Luzon Strait, which means the model drifting is small. Recent studies indicated that the deep upwelling near the deep west boundary and seamounts may also be driven by near-boundary mixing (e.g., Ferrari et al., 2016; Mcdougall and Ferrari, 2017).

In the present study, the deep circulation in the SCS is investigated by mesoscale-eddy-resolving model simulations, and found to be in reasonable agreement with mooring arrays. Analysis of these results provides a detailed structure and variability of the deep circulation in the SCS. The major features of the SCS deep circulation are a basin-scale cyclonic gyre and a western intensification. The transport of the DWBC is ~2 Sv at 16.5 ℃N with a width of ~53 km. Flowing southwestward, the DWBC becomes weaker and gets a wider range. By dividing the differences between transports with corresponding areas, the values of upwelling are from 0.19 to 0.36 m d^{-1}, with the strongest area being around the DWBC. The model results reveal the existence of an 80- to 120-day oscillation in the deep northeastern circulation and the DWBC, which are also the large mean EKE areas. This intraseasonal oscillation has a northwestward direction, with a velocity amplitude of ~1.0 to 1.5 cm s^{-1} in zonal and meridional velocity. The distribution of mixing parameters in the deep SCS plays a role in both the spatial structure and volume transport of the deep circulation. Comparing the northern shelf of the SCS with the Luzon Strait, deep circulation in the SCS is more sensitive to the large vertical mixing parameters in the Zhongsha Island Chain area. Even though the model is idealized, the model current fields qualitatively reproduce the results of direct current measurement and open new routes to understand the dynamic that mixing regulating deep circulation. The success of the present model may be associated with several intrinsic features of the deep circulation. It is noteworthy that despite reasonable agreement between the current simulation and observations, surface forcing, which have potential impact on the modification of ocean stratification and the deep circulation (e.g., Su et al., 2014, 2016a, 2016b; Yang et al., 2015), is not applied to the numerical experiments. Although configured with a buffer zone near the eastern boundary, the experiments are currently configured with closed lateral boundary condition, which cannot simulate the interactions between the processes of the current model domain and the Pacific/Indonesia seas. These limitations may introduce uncertainty to some extent to the simulation results in this study. The potential impact of surface forcing and boundary conditions on the deep circulation in the SCS is worth to be investigated.

Data availability

Model outputs are available upon request to the first author.

Author contribution

All the authors conceived and designed the experiments and contributed ideas in the writing process. X.Z. performed the experiments, analyzed the data and wrote the paper.

Acknowledgements

This work was supported by the National Key Research and Development Program of China (Grant no. 2016YFC1402605), the National Natural Science Foundation of China (Grant nos. 41676011, 41806031, 41606014, 91628302), the National Key Research and Development Program of China (Grant no. 2018YFC1407002, 2016YFC1402103), the East Asia Marine Cooperation Platform (China-ASEAN marine cooperation fund), the National Key Basic Research Program of China (Grant no. 2014CB745003), the Global Change and Air–Sea Interaction Project (Grant nos. GASI-IPOVAI-01-03, GASI-IPOVAI-01-02), the Foundation for Innovative Research Groups of the National Natural Science Foundation of China (Grant no. 41521091), the Key Research and Development Program of Shandong (Grant no. 2016CYJS02A03), and the NSFC-Shandong Joint Fund for Marine Science Research Centers (Grant no. U1406401).

References

Alford, M. H., MacKinnon, J. A., Nash, J. D., Simmons, H., Pickering, A., Klymak, J. M., Pinkel, R., Sun, O., Rainville, L., Musgrave, R., Beitzel, T., Fu, K.-H., and Lu, C.-W.: Energy flux and dissipation in Luzon Strait: two tales of two ridges, J. Phys. Oceanogr., 41, 2211-2222, doi:10.1175/JPO-D-11-073.1, 2011.

Anderson, D. and Gill, A.: Spin-up of a stratified ocean, with application to upwelling, Deep Sea Res. Oceanogr. Abstr., 22, 593-596, 1975.

Bleck, R.: An oceanic general circulation model framed in hybrid isopycnic-Cartesian coordinates, Ocean Modell., 37, 55-88, doi:10.1016/S1463–5003(01)00012-9, 2002.

Carnes, M. R.: Description and evaluation of GDEM-V3.0. Naval Research Laboratory Tech, Rep. NRL/MR/7330-09-9165, 21, available online at http://www7320.nrlssc.navy.mil/pubs/2009/carnes-2009.pdf, 2009.

Chang, Y.-T., Hsu, W.-L., Tai, J.-H., Tang, T.-Y., Chang, M.-H., and Chao, S.-Y.: Cold deep water in the South China Sea, J. Oceanogr., 66, 183-190, doi:10.1007/s10872-010-0016-x, 2010.

Chao, S.-Y., Shaw, P. T., and Wu, S. Y.: Deep water ventilation in the South China Sea, Deep-Sea Res. I, 43, 445-466, 1996.

Chassignet, E. P., Smith, L. T., Halliwell, G. R., and Bleck, R.: North Atlantic simulations with the hybrid coordinate ocean model (HYCOM): Impact of the vertical coordinate choice, reference pressure, and thermobaricity, J. Phys. Oceanogr., 33, 2504-2526, doi:10.1175/1520-0485(2003)033<2504:NASWTH>2.0.CO;2, 2003.

Chen, C.-T. and Huang, M. H.: A mid-depth front separating the South China Sea Water and the Philippine Sea Water, J. Oceanogr., 52, 17-25, doi:10.1007/BF02236530, 1996.

Endoh, T. and Hibiya, T.: Numerical study of the meridional overturning circulation with ‘‘mixing hotspots’’ in the Pacific Ocean, J. Oceanogr., 62, 259-266, doi:10.1007/s10872-006-0050-x, 2006.

Ferrari, R., Mashayek, A., McDougall, T. J., Nikurashin, M., and Campin, J.-M.: Turning ocean mixing upside down, J. Phys. Oceanogr., 46, 2239-2261, doi:10.1175/JPO-D-15-0244.1, 2016.

Forget, G., Campin, J.-M., Heimbach, P., Hill, C. N., Ponte, R. M., and Wunsch, C.: ECCO version 4: An integrated framework for non-linear inverse modeling and global ocean state estimation, Geosci. Model Dev. 8, 3071-3104, doi:https://doi.org/10.5194/gmd-8-3071-2015, 2015.

Furue, R. and Endoh, M.: Effects of the Pacific diapycnal mixing and wind stress on the global and Pacific meridional overturning circulation, J. Phys. Oceanogr., 35, 1876-1890, doi:10.1175/JPO2792.1, 2005.

Gan, J., Liu, Z., and Hui, C.: A three-layer alternating spinning circulation in the South China Sea, J. Phys. Oceanogr., 46, 2309-2315, doi:10.1175/JPO-D-16-0044.1, 2016.

Gordon, A. L., Huber, B. A., Metzger, E. J., Susanto, R. D., Hurlburt, H. E., and Adi, T. R.: South China Sea Throughflow impact on the Indonesian Throughflow, Geophys. Res. Lett., 39, L11602, doi:10.1029/2012GL052021, 2012.

Hamilton, P.: Topographic Rossby waves in the Gulf of Mexico, Progr. Oceanogr., 82, 1-31, doi:10.1016/j.pocean.2009.04.019, 2009.

Jan, S., Chern, C.-S., Wang, J., and Chao, S.-Y.: Generation of diurnal K1 internal tide in the Luzon Strait and its influence on surface tide in the South China Sea, J. Geophys. Res., 112, C06019, doi:10.1029/2006JC004003, 2007.

Johns, W. E. and Watts, D. R.: Time Scales and structure of topographic Rossby waves and meanders in the deep Gulf Stream, J. Mar. Res., 44, 267-290, 1986.

Kunze, E., Firing, E., Hummon, J. M., Chereskin, T. K., and Thurnherr, A. M.: Global abyssal mixing inferred from lowered ADCP shear and CTD strain profiles, J. Phys. Oceanogr., 36, 1553-1576, doi:10.1175/JPO2926.1, 2006.

Lan, J., Zhang, N., and Wang, Y.: On the dynamics of the South China Sea deep circulation, J. Geophys. Res. Oceans, 118, 1206-1210, doi:10.1002/jgrc.20104, 2013.

Lan, J., Wang, Y., Cui, F., and Zhang, N.: Seasonal variation in the South China Sea deep circulation, J. Geophys. Res. Oceans, 120, 1682-1690, doi:10.1002/2014JC010413, 2015.

Large, W. G., McWilliams, J. C., and Doney, S. C.: Ocean vertical mixing: A review and a model with a nonlocal boundary layer parameterization, Rev. Geophys., 32, 363-403, doi:10.1029/94RG01872, 1994.

Li, L. and Qu, T.: Thermohaline circulation in the deep South China Sea basin inferred from oxygen distributions, J. Geophys. Res., 111, C05017, doi:10.1029/2005JC003164, 2006.

Liu, C.-T. and Liu, R.-J.: The deep current in the Bashi Channel, Acta Oceanogr. Taiwan, 20, 107-116, 1988.

Mantyla, A. W.: On the potential temperature in the abyssal Pacific Ocean, J. Mar. Res., 33, 341-353, 1975.

Mcdougall T. J. and Ferrari, R.: Abyssal upwelling and downwelling driven by near-boundary mixing, J. Phys. Oceanogr., 47, 261-283, doi:10.1175/JPO-D-16-0082.1, 2017.

Niwa, Y. and Hibiya, T.: Three-dimensional numerical simulation of M2 internal tides in the East China Sea, J. Geophys. Res., 109, C04027, doi:10.1029/2003JC001923, 2004.

Platzman, G. W.: Two-dimensional free oscillations in natural basins, J. Phys. Oceanogr., 2, 117-138, 1972.

Pickart, R. S. and Watts, D. R.: Deep western boundary current variability at Cape Hatteras, J. Mar. Res., 48, 765-791, 1990.

Polzin, K. L., Speer, K. G., Toole, J. M., and Schmitt, R. W.: Intense mixing of Antarctic bottom water in the equatorial Atlantic Ocean. Nature, 380(6569): 54-57, doi:10.1038/380054a0, 1996.

Qu, T., Mitsudera, H., and Yamagata, T.: Intrusion of the North Pacific waters in the South China Sea, J. Geophys. Res., 105, 6415-6424, doi:10.1029/1999JC900323, 2000.

Qu, T., Girton, J. B., and Whitehead, J. A.: Deepwater overflow through Luzon Strait, J. Geophys. Res., 111, C01002, doi:10.1029/2005JC003139, 2006a.

Qu, T., Du, Y., and Sasaki, H.: South China Sea throughflow. A heat and freshwater conveyor, Geophys. Res. Lett., 33, L23617, doi:10.1029/2006GL028350, 2006b.

Qu, T., Song, T., and Yamagata, T.: An introduction to the South China Sea throughflow: Its dynamics, variability, and implication for climate, Dyn. Atmos. Oceans, 47, 3-14, doi:10.1016/j.dynatmoce.2008.05.001, 2009.

Rhines, P.: Edge-, bottom- and Rossby wave in a rotating straitified fluid, Geophys. Fluid Dyn., 1, 273-302, 1970.

Shu, Y., Xue, H., Wang, D., Chai, F., Xie, Q., Yao, J., and Xiao, J.: Meridional overturning circulation in the South China Sea envisioned from the high-resolution global reanalysis data GLBa0.08, J. Geophys. Res. Oceans, 119, 3012-3028, doi:10.1002/2013JC009583, 2014.

Smith, W. H. F. and Sandwell, D. T.: Global seafloor topography from satellite altimetry and ship depth soundings, Science, 277, 1956-1962, doi:10.1126/science.277.5334.1956, 1997.

Song, Y.T.: Estimation of inter basin transport using ocean bottom pressure: Theory and model for Asian marginal seas, J. Geophys. Res., 111, C11S19, doi:10.1029/2005JC003189, 2006.

Stommel, H. and Arons, A. B.: On the abyssal circulation of the world ocean-I. Stationary planetary flow patterns on a sphere, Deep-Sea Res. I, 6, 140-154, doi:10.1016/0146-6313(59)90065-6, 1960a.

Stommel, H. and Arons, A. B.: On the abyssal circulation of the world ocean-II. An idealized model of the circulation pattern and amplitude in oceanic basins, Deep-Sea Res. I, 6, 217-233, doi:10.1016/0146-6313(59)90075-9, 1960b.

Su, Z., Stewart A., and Thompson A.: An idealized model of Weddell Gyre export variability, J. Phys. Oceanogr., 44, 1671-1688, doi:10.1175/JPO-D-13-0263.1, 2014.

Su, Z., Ingersoll, A. P., Stewart, A. L., and Thompson, A. F.: Ocean convective available potential energy. Part II: Energetics of thermobaric convection and thermobaric cabbeling, J. Phys. Oceanogr., 46, 1097-1115, doi:10.1175/JPO-D-14-0156.1, 2016a.

Su, Z., Ingersoll, A. P., and He, F.: On the abruptness of Bølling–Allerød warming, J. Climate, 29, 4965-4975, doi:10.1175/JCLI-D-15-0675.1, 2016b.

Su, Z. and Ingersoll, A. P.: On the minimum potential energy state and the eddy-size-constrained APE density, J. Phys. Oceanogr., 46, 2663-2674, doi:10.1175/JPO-D-16-0074.1, 2016.

Su, Z., Wang, J., Klein, P., Thompson, A. F., and Menemenlis, D.: Ocean submesoscales as a key component of the global heat budget, Nature Communications, 9(1), 775, doi:10.1038/s41467-018-02983-w, 2018.

Thompson, R. O. R. Y.: Observations of Rossby waves near Site D, Prog. in Oceanogr., 7, 1-28, 1977.

Tian, J., Zhou, L., Zhang, X., Liang, X., Zheng, Q., and Zhao, W.: Estimates of M2 internal tide energy fluxes along the margin of Northwestern Pacific using TOPEX/POSEIDON altimeter data, Geophys. Res. Lett., 30, 1889, doi:10.1029/2003GL018008, 2003.

Tian, J., Yang, Q., Liang, X., Xie, L., Hu, D., Wang, F., and Qu, T.: Observation of Luzon Strait transport, Geophys. Res. Lett., 33, L19607, doi:10.1029/2006GL026272, 2006.

Tian, J., Yang, Q., and Zhao, W.: Enhanced diapycnal mixing in the South China Sea, J. Phys. Oceanogr., 39, 3191-3203, doi:10.1175/2009JPO3899.1, 2009.

Tian, J. and Qu, T.: Advances in research on the deep South China Sea circulation, Chin. Sci. Bull., 57, 3115-3120, doi:10.1007/s11434-012-5269-x, 2012.

Wang, J.: Observation of abyssal flows in the Northern South China Sea, Acta Oceanogr. Taiwan, 16, 36-45, 1986.

Wang, G., Xie, S.-P., Qu, T., and Huang, R. X.: Deep South China Sea circulation, Geophys. Res. Lett., 38, L05601, doi:10.1029/2010GL046626, 2011.

Wang, X., Liu, Z., and Peng, S.: Impact of Tidal Mixing on Water Mass Transformation and Circulation in the South China Sea, J. Phys. Oceanogr., 47, 419-432, doi:10.1175/JPO-D-16-0171.1, 2017.

Wyrtki, K.: Physical oceanography of the southeast Asian Waters, Naga Rep., 2, 195, Scripps Inst. of Oceanogr. San Diego, Calif, 1961.

Xu, F. and Oey, L. Y.: State analysis using the Local Ensemble Transform Kalman Filter (LETKF) and the three-layer circulation structure of the Luzon Strait and the South China Sea, Ocean. Dynam., 64, 905-923, doi:10.1007/s10236-014-0720-y, 2014.

Xu, Y., Rolph, W. D., Mark, W., and Jae-Hun, P.: Fundamental-mode basin oscillations in the japan/east sea, Geophys. Res. Lett., 34(4), 545-559, 2007.

Yang, J.: Local and remote wind stress forcing of the seasonal variability of the Atlantic Meridional Overturning Circulation (AMOC) transport at 26.5 °N, J. Geophys. Res. Oceans, 120(4): 2488-2503, doi:10.1002/2014JC010317, 2015.

Yang, Q., Tian, J., and Zhao, W.: Observation of Luzon Strait transport in summer 2007, Deep-Sea Res. I, 57, 670-676, doi:10.1016/j.dsr.2010.02.004, 2010.

Yang, Q., Tian, J., and Zhao, W.: Observation of material fluxes through the Luzon Strait, Chin. J. Oceanol. Limnol., 29, 26-32, doi:10.1007/s00343-011-9952-6, 2011.

Yang, Q., Zhao, W., Liang, X., and Tian, J.: Three-dimensional distribution of turbulent mixing in the South China Sea, J. Phys. Oceanogr., 46, 769-788, doi:10.1175/JPO-D-14-0220.1, 2016.

Yaremchuk, M., McCreary, Jr. J., Yu, Z., and Furue, R.: The South China Sea throughflow retrieved from climatological data, J. Phys. Oceanogr., 39, 753-767, doi:10.1175/2008JPO3955.1, 2009.

Ye, R., Zhou C., Zhao W., Tian J., Yang Q., Huang X., Zhang Z., and Zhao X.: Variability in the Deep Overflow through the Heng-Chun Ridge of the Luzon Strait, J. Phys. Oceanogr., 49, 811-825, https://doi.org/10.1175/JPO-D-18-0113.1, 2019.

Yu, X., Naveira Garabato, A. C., Martin, A. P., Buckingham, C. E., Brannigan, L., and Su, Z.: An annual cycle of submesoscale vertical flow and restratification in the upper ocean, J. Phys. Oceanogr., 1439-1461, doi:10.1175/JPO-D-18-0253, 2019.

Zhao, W., Zhou, C., Tian, J., Yang, Q., Wang, B., Xie, L., and Qu, T.: Deep water circulation in the Luzon Strait, J. Geophys. Res., 119, 790-804, doi:10.1002/2013JC009587, 2014.

Zhao, X., Zhou, C., Zhao, W., Tian, J., and Xu, X.: Deepwater overflow observed by three bottom-anchored moorings in the Bashi Channel, Deep-Sea Res. I, 110, 65-74, doi:10.1016/j.dsr.2016.01.007, 2016.

Zhang, Z., Zhao, W., Tian, J., Yang, Q., and Qu, T.: Spatial structure and temporal variability of the zonal flow in the Luzon Strait, J. Geophys. Res., 120, 759-776, doi:10.1002/2014JC010308, 2015.

Zhou, C., Zhao, W., Tian, J., Yang, Q., and Qu, T.: Variability of the deep-water overflow in the Luzon Strait, J. Phys. Oceanogr., 44, 2972-2986, doi:10.1175/JPO-D-14-0113.1, 2014.

Zhou, C., Zhao, W., Tian, J., Zhao, X., Zhu, Y., Yang, Q., and Qu, T.: Deep western boundary current in the South China Sea, Sci. Rep., 7, 9303, doi:10.1038/s41598-017-09436-2, 2017.

Zhou, C., Zhao, W., Tian, J., Yang, Q., Huang, X., Zhang, Z., and Qu, T.: Observations of Deep Current at the Western Boundary of the Northern Philippine Basin, Sci. Rep., 8, 14334, doi:10.1038/s41598-018-32541-9, 2018.

469 Table 1. Mooring configurations with mean zonal and meridional velocities in different depths.

Mooring ID	Longitude [°E]	Latitude [°N]	Water depth [m]	Current meter depth [m]	$\overline{U}$ [cm s^{-1}]	$\overline{V}$ [cm s^{-1}]
M1	114°35.761'	15°14.855'	3560	1940	-0.47	-0.07
				2440	-1.11	-0.39
				2940	-1.14	-1.08
				3440	-0.58	-0.51
M2	114°42.094'	15°11.961'	4282	2062	-0.15	-0.22
				2562	-0.27	-0.45
				3062	-0.48	-0.76
				3562	-0.64	-1.21
				4062	-0.78	-1.85
M3	115°07.607'	14°56.235'	4281	2061	0.02	-0.21
				2561	0.22	-0.28
				3061	0.10	-0.40
				3561	-0.30	-0.44
				4061	-0.27	-0.58
M4	115°20.954'	14°52.977'	4200	1980	0.11	0.07
				2480	0.32	0.62
				2980	0.44	0.76
				3480	0.63	0.53
				3980	0.19	0.39
M5	115°51.996'	14°50.133'	4266	2046	-0.53	0.23
				2546	-0.35	0.32
				3046	-0.30	0.22
				3546	-0.16	0.03
				4046	-0.64	0.24
M6	116°03.241'	14°53.750'	4286	2066	-1.33	0.55
				2566	-0.96	0.42
				3066	-1.10	0.02
				3566	-1.39	-0.36
				4066	-1.80	-0.73

470

471

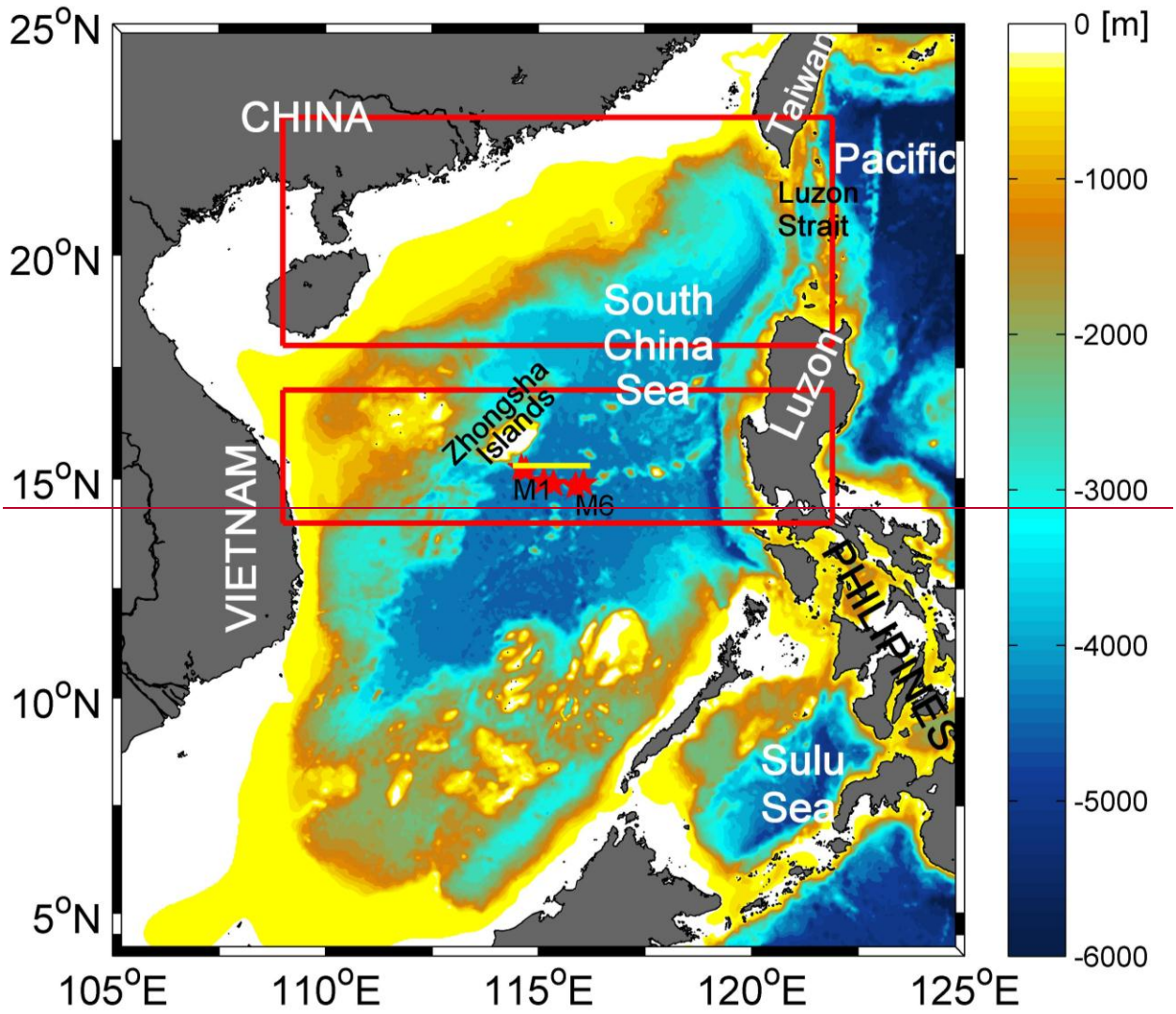
25°N
20°N
15°N
10°N
5°N
105°E
110°E
115°E
120°E
125°E
CHINA
Taiwan
Pacific
Luzon Strait
South China Sea
Zhongsha Islands
M1
M6
Luzon
VIETNAM
PHILIPPINES
Sulu Sea
0 [m]
-1000
-2000
-3000
-4000
-5000
-6000

472

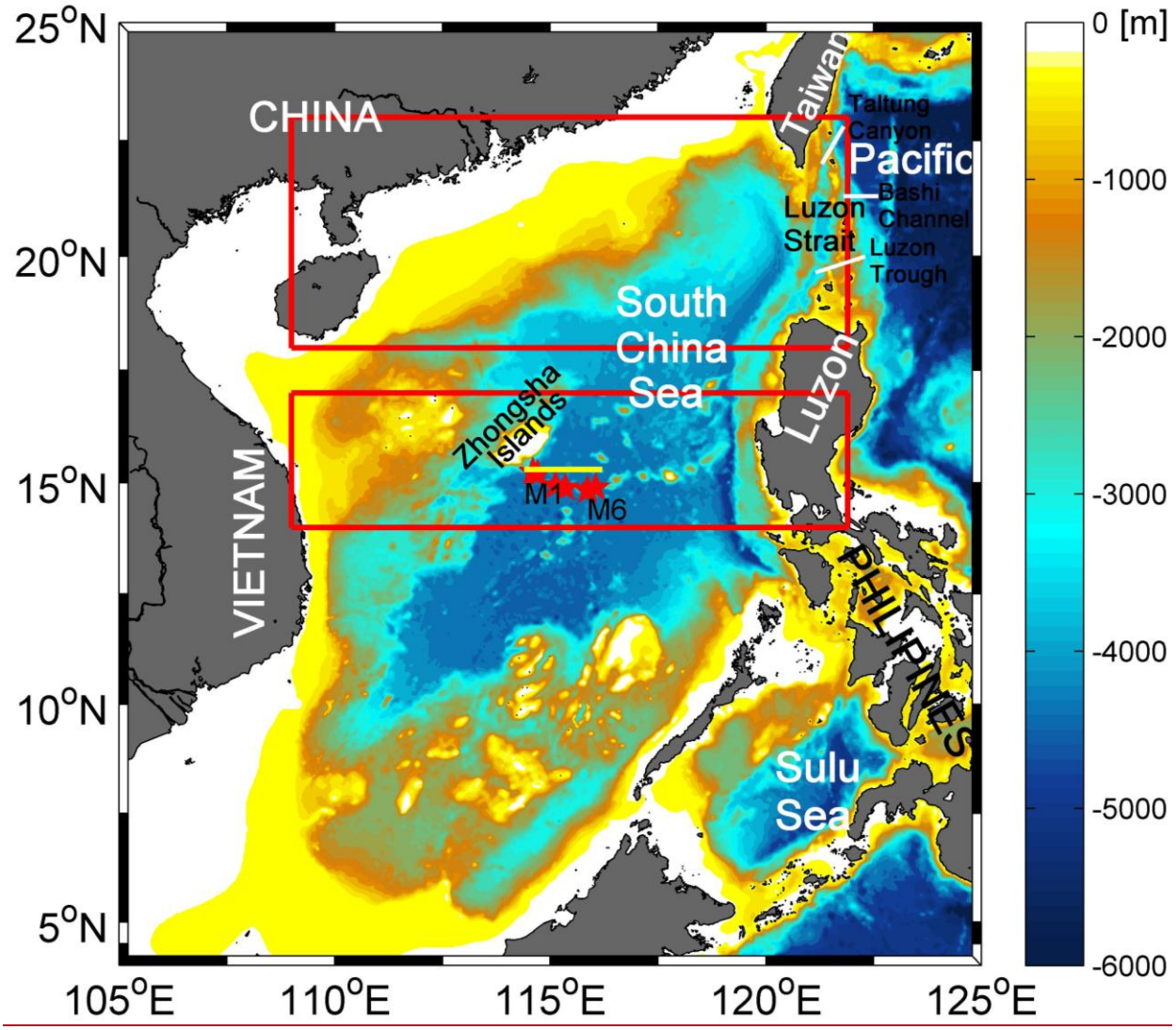

Figure 1. Bottom topography of the South China Sea. The red stars denote the locations of the year-long mooring array M1-M6. The yellow line indicates the location of model section shown in Fig. ~~2b~~3b. Red boxes indicate the areas with strong mixing in the control run based on Yang et al. (2016).

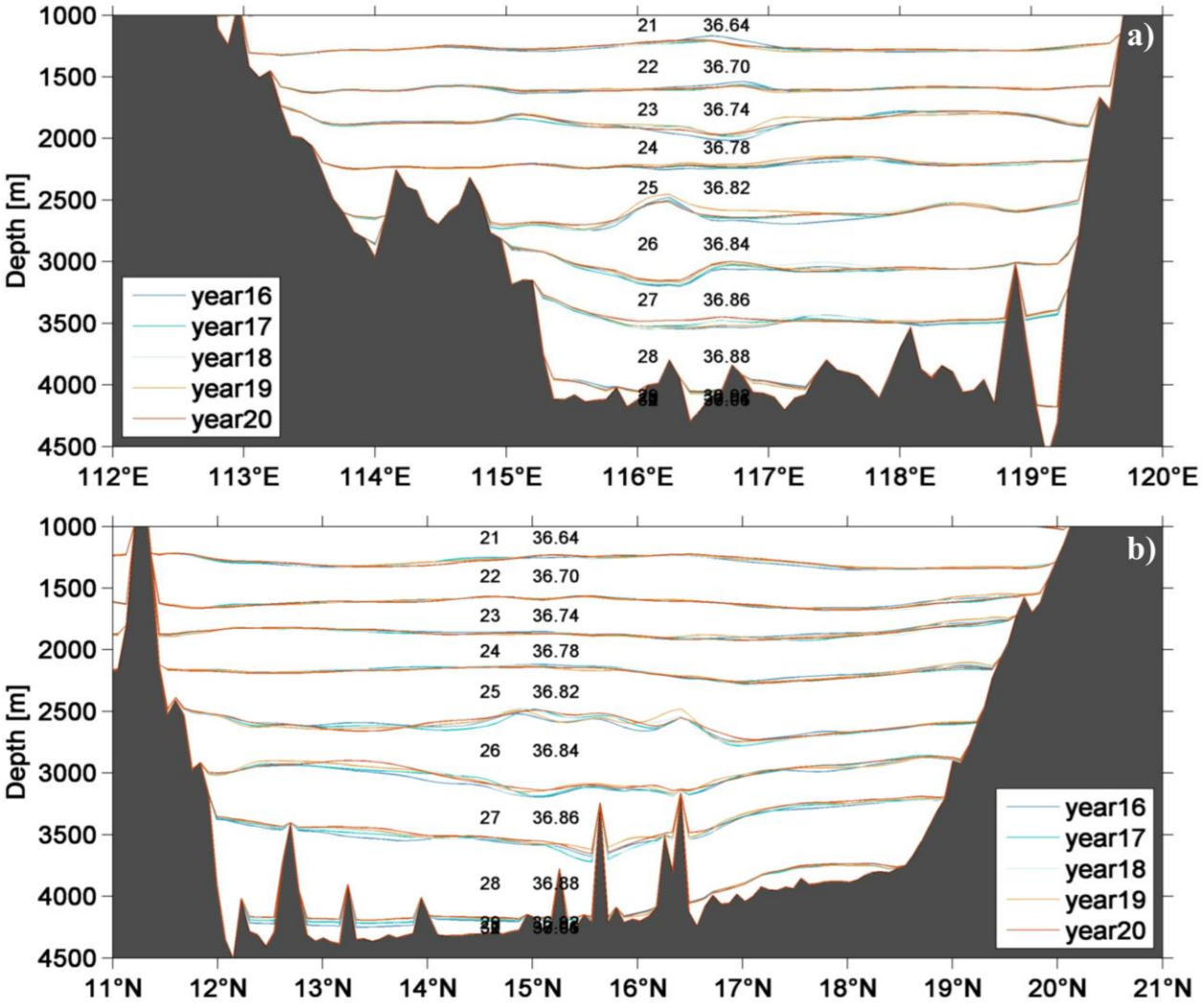

478

479 **Figure 2. Section view of year-mean thickness structure at a zonal section of 16.5 ℃N (a) and a meridional section of 116 ℃E**
480 **(b) for the control run. Thickness numbers and density referenced to 2000 m (σ_2, kg m^{-3}) are indicated.**

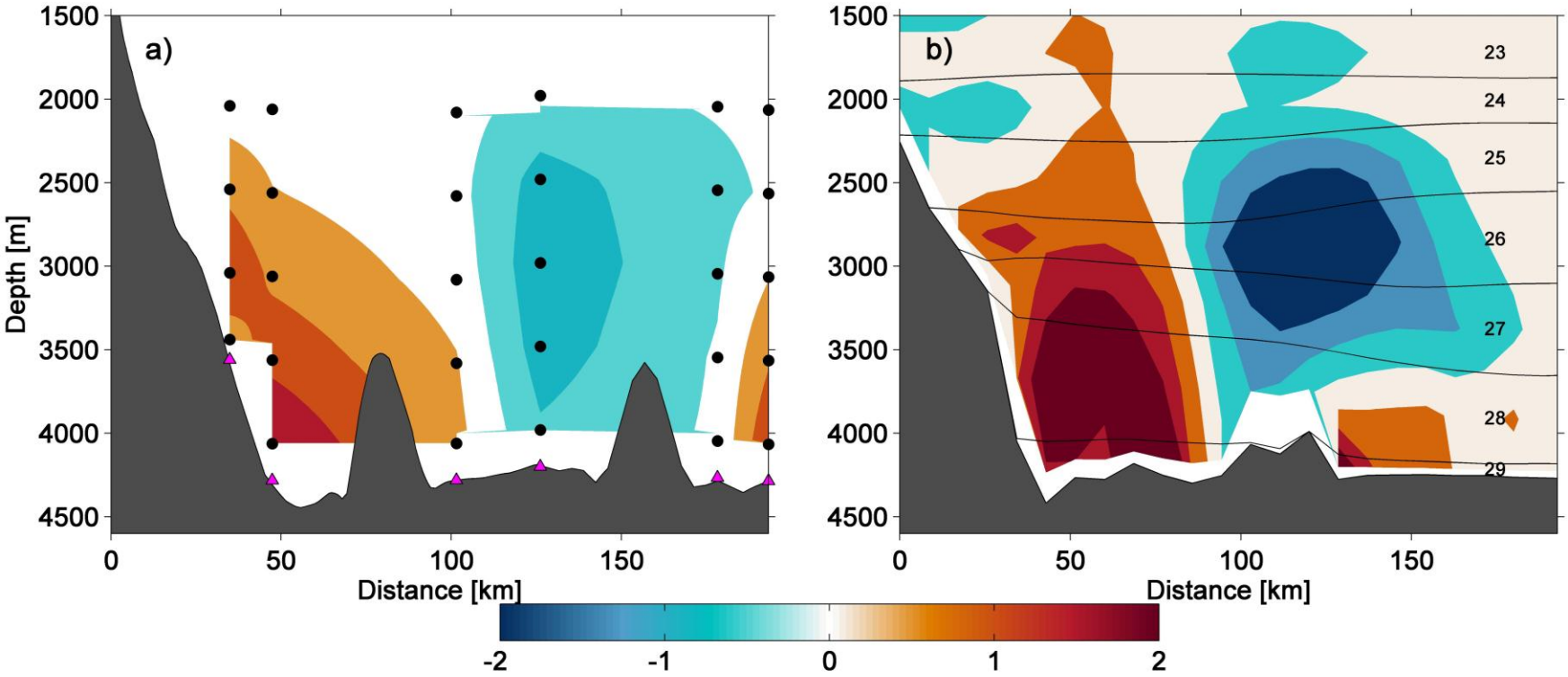

481

482 **Figure ~~2~~3. a) Section view of observed mean cross-section velocity (in cm s^{-1}) from Zhou et al. (2017; their Fig. 2a). Mooring locations are indicated in magenta triangles.**
483 **Locations of current meters are indicated by black dots. b) Time-mean structure of velocity (in cm s^{-1}) and thickness numbers at a zonal section of 15.4 ℃N for the control**
484 **run. Note the positive value represents southward velocity.**

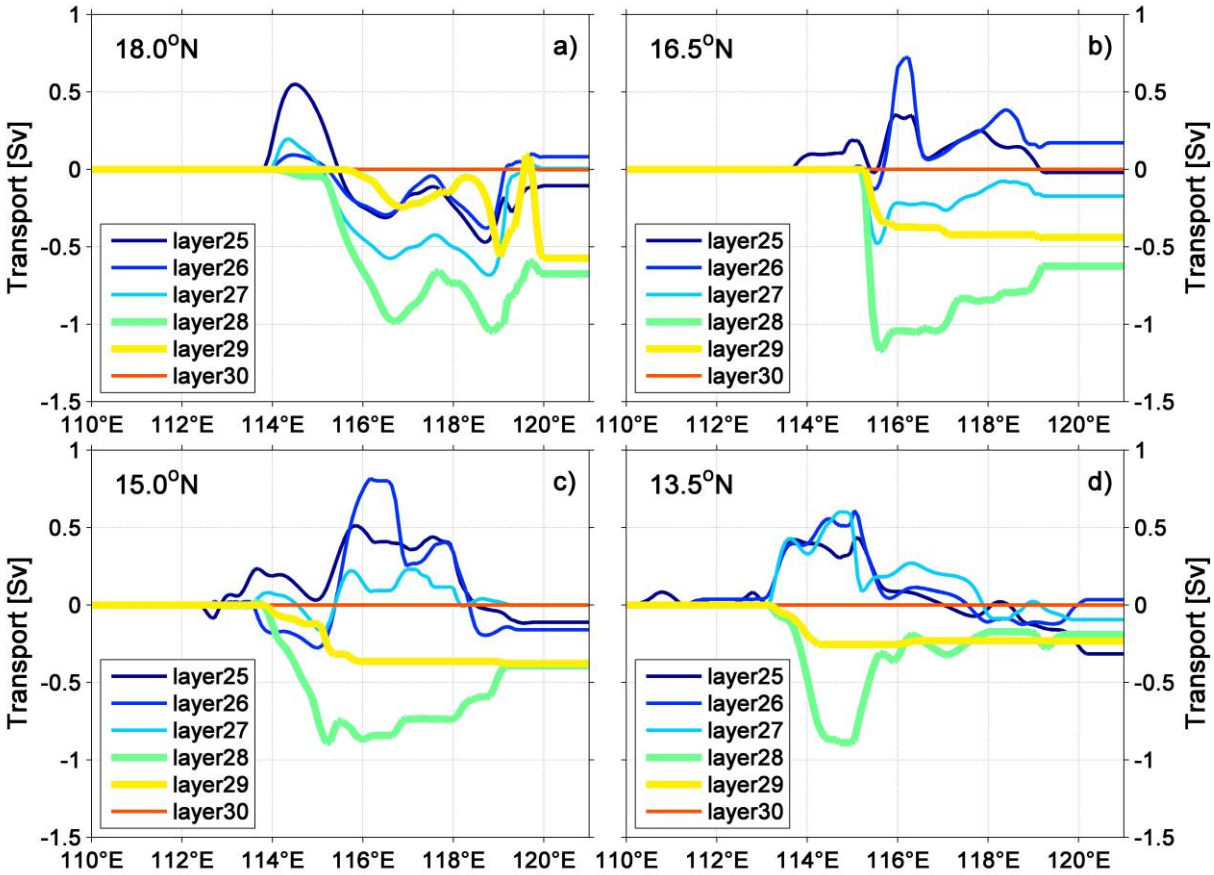

Figure ~~3~~4. Eastward cumulated of the meridional volume transports (in Sv) across the model section along 4 zonal sections (13.5 ℃N, 15.0 ℃N, 16.5 ℃N and 18.0 ℃N) of each layer from the 25th to 30th from 110 ℃E to 121 ℃E for the control run. The negative value represents southward volume transport. The depth of the isopycnic interfaces are indicated in Fig. 2b.

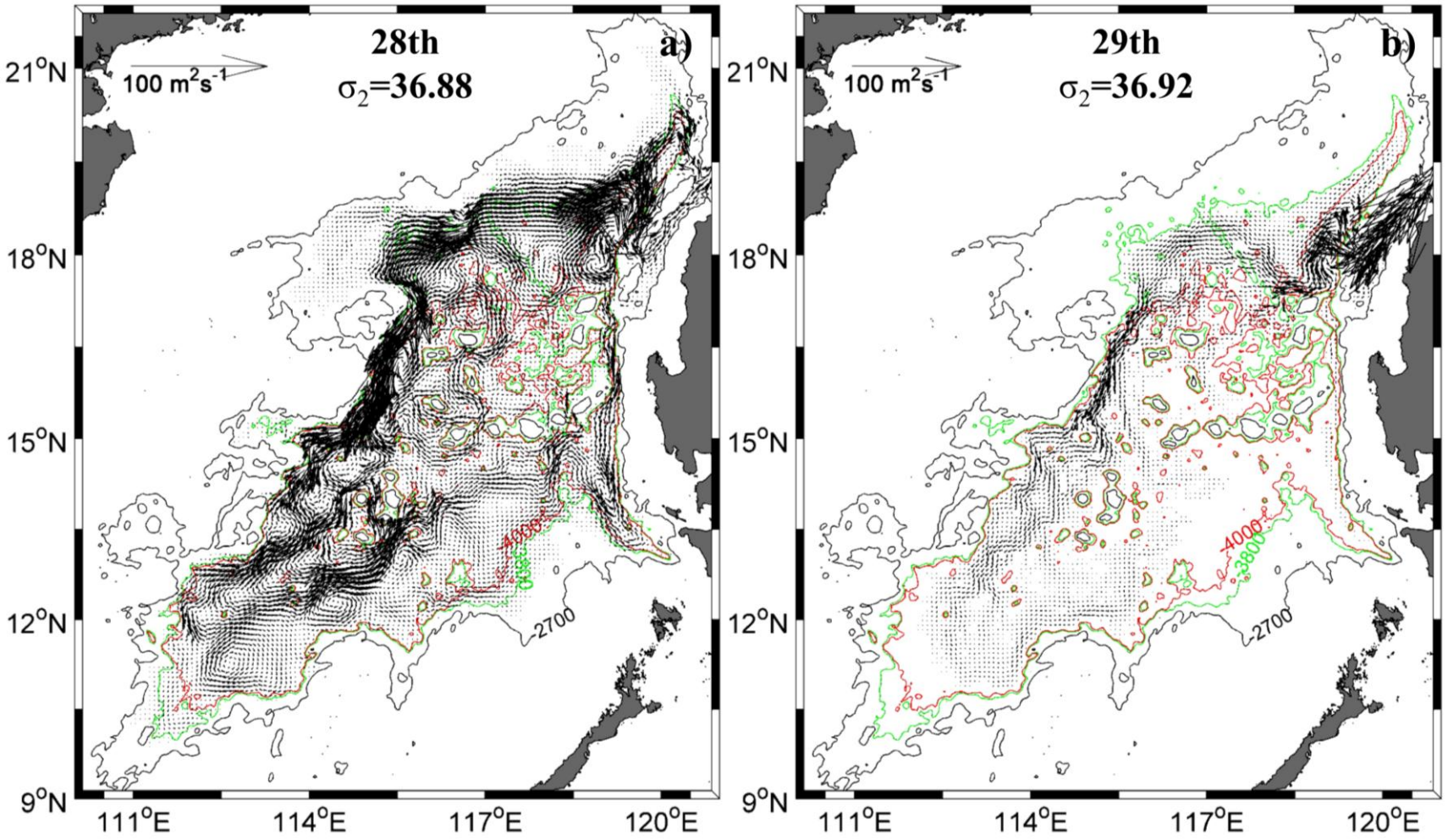

489

490 **Figure 45. Mean volume transport per unit width (in m^2 s^{-1}) of the 28th (a) and 29th layer (b) for the control run.**

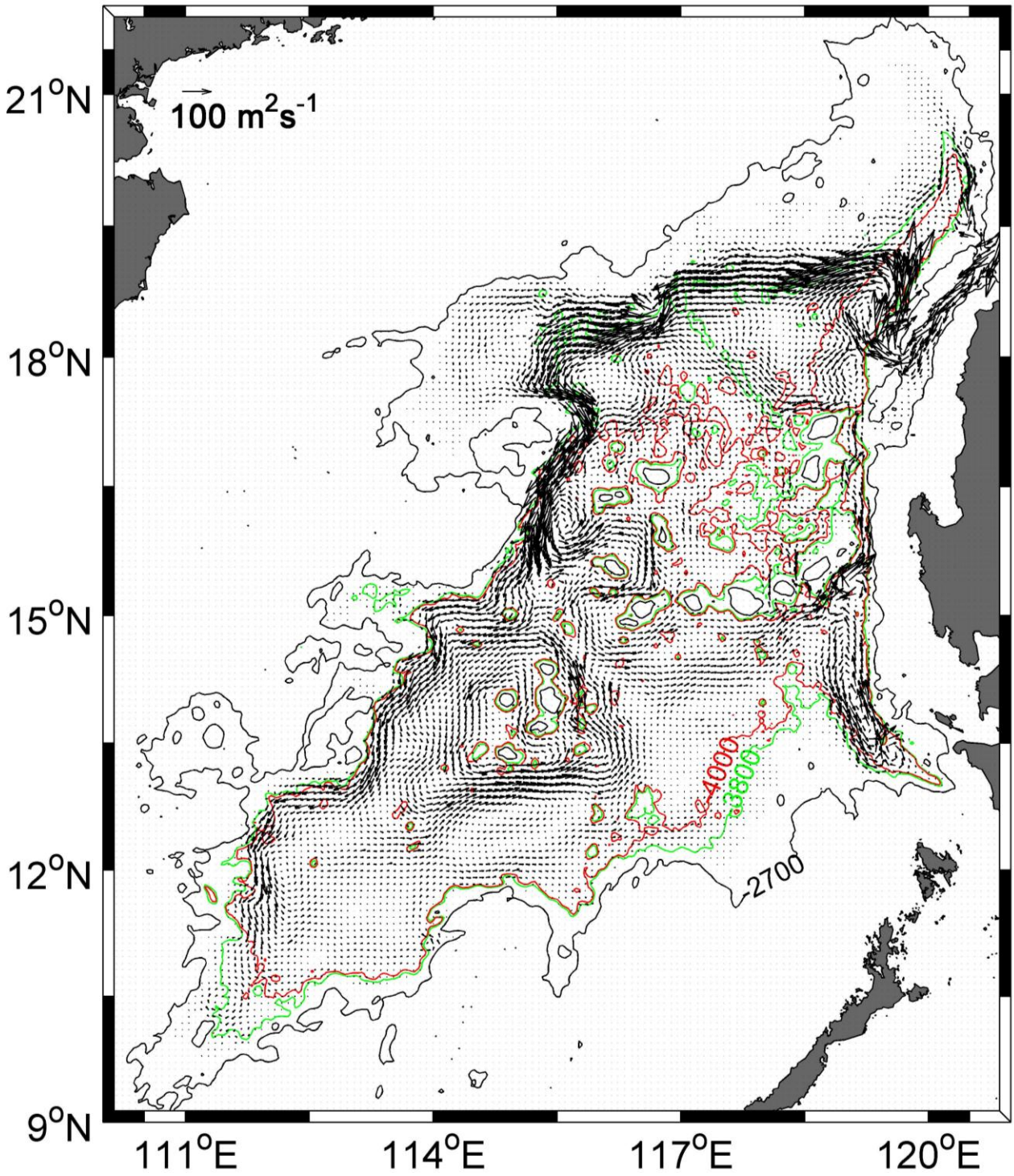

491

492 **Figure ~~5~~6. Total ~~M~~mean volume transport per unit width (in $m^2 s^{-1}$) ~~from~~of the 28th ~~to~~and 29th layer for the control run.**

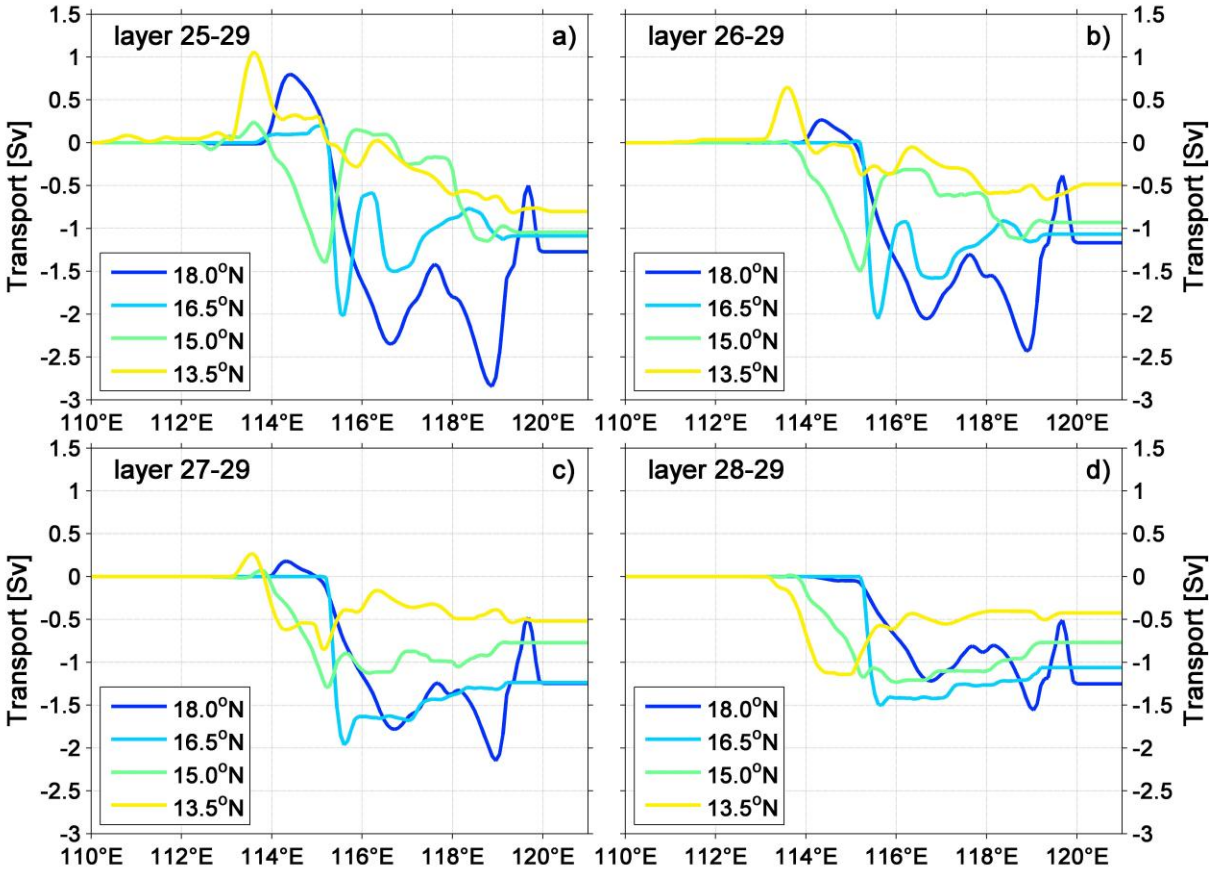

493

494 **Figure ~~6~~7. Eastward cumulated of the meridional volume transports (in Sv) across the model section along 4 zonal**
495 **sections (13.5 ℃N, 15.0 ℃N, 16.5 ℃N and 18.0 ℃N) from different layers to 29th from 110 ℃E to 121 ℃E for the control run. The**
496 **negative value represents southward volume transport.**

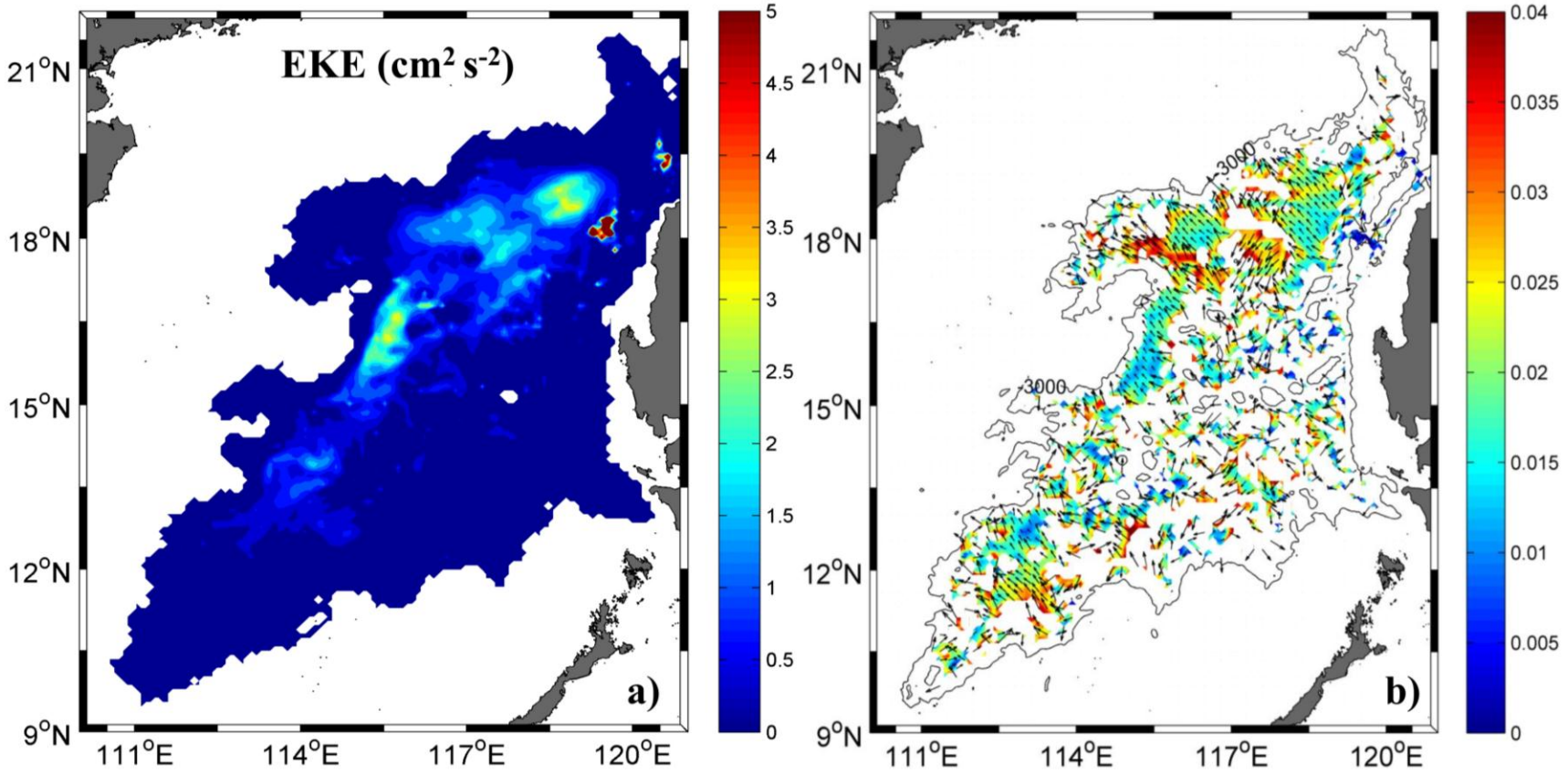

497

498 **Figure ~~7~~8. Distribution of modeled eddy kinetic energy EKE (a, in cm^2 s^{-2}) in the South China Sea, mean phase speed and direction of propagation (b, in m s^{-1}) from the**
499 **28th to 29th layer for the control run.**

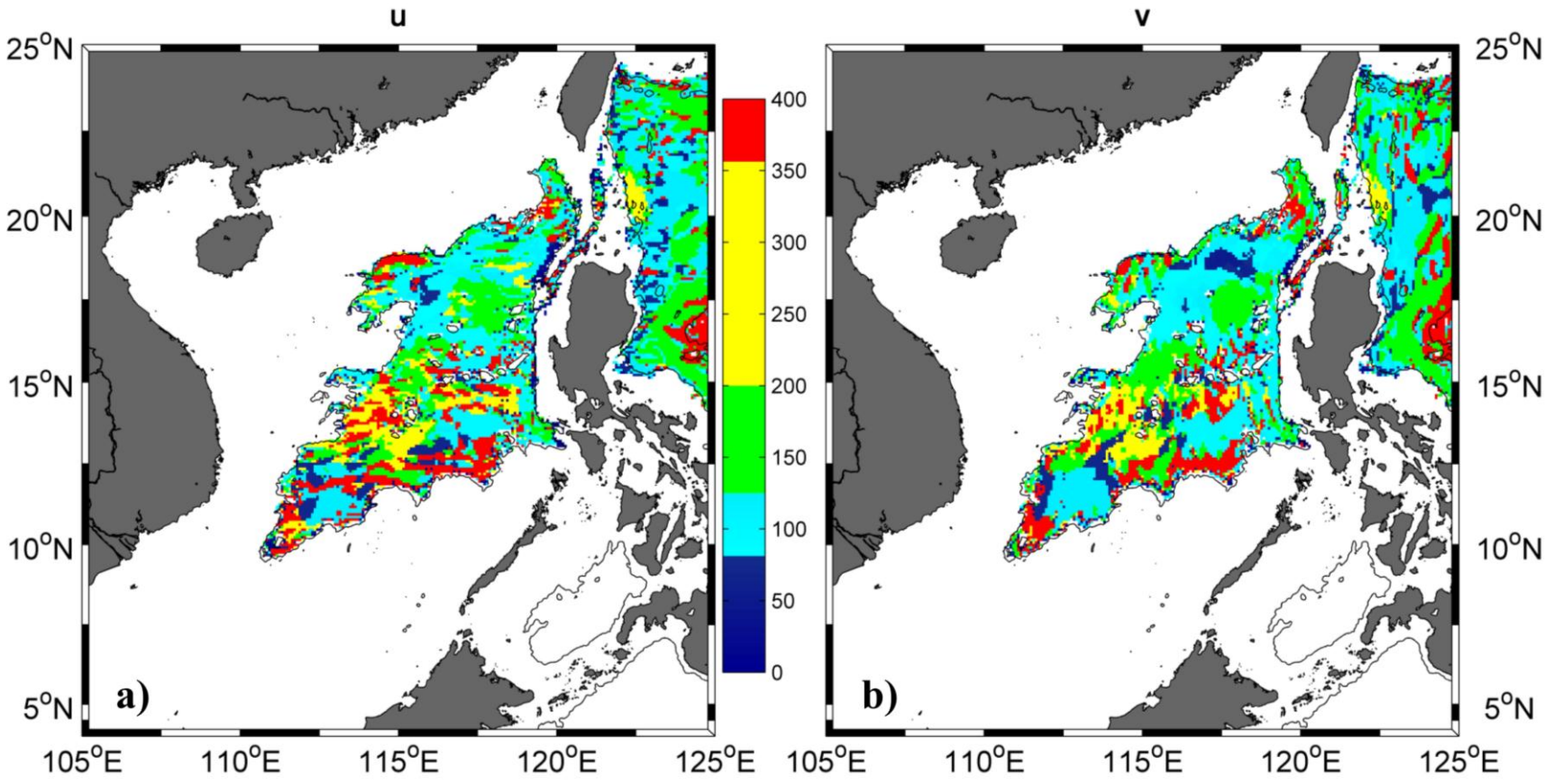

500

501 **Figure ~~8~~9. Periods (in days) of max power spectra density (PSD) of zonal (a) and meridional (b) velocity from the 28th to 29th layer at each gird point for the control run.**

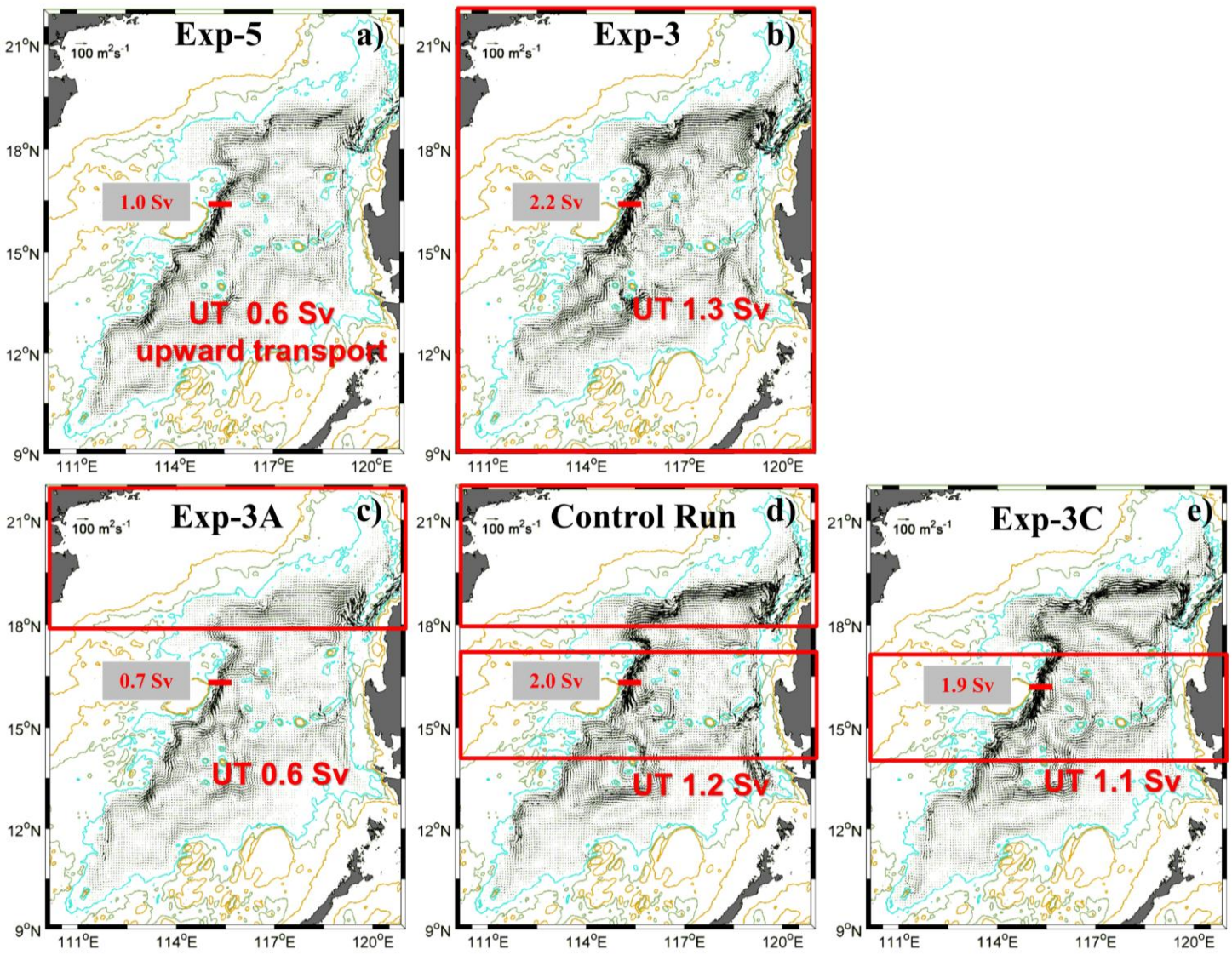

Figure ~~9~~10. Total ~~M~~mean volume transport per unit width (in $m^2\ s^{-1}$) ~~from~~of the 28th ~~to~~and 29th layer in Exp-5, Exp-3, Exp-3A, control Run, and Exp-3C. The cross sections are indicated by red lines and the corresponding volume transports (in Sv) are indicated in the textboxes with gray background. Red boxes indicate the areas with strong mixing.

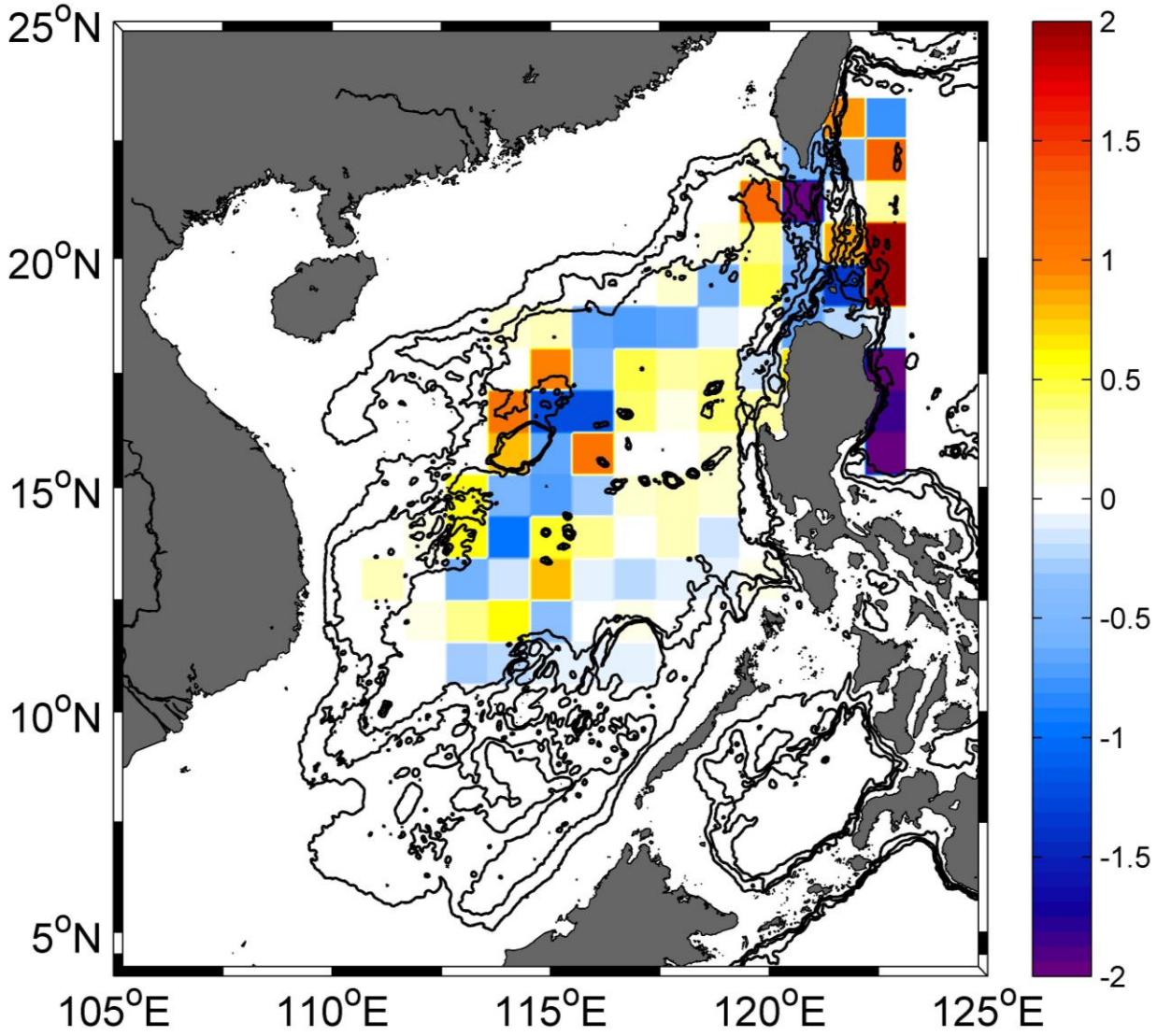

Figure ~~10~~11. Horizontal distribution of diapycnal water mass transformation (in m d^{-1}) binned in 1 °×1 °cells across upper interface of the 28th layer for the control run.